Supporting Information

Additive-free Molecular Acceptor Organic Solar Cells Processed from a Biorenewable Solvent Approaching 15% Efficiency

Zhifang Du[1], *Hoang Mai Luong*[1], *Sina Sabury*[2], *Pattarawadee Therdkatanyuphong*[3], *Sangmin Chae*[1], *Claire Welton*[4], *Austin L. Jones*[2], *Junxiang Zhang*[3], *Zhengxing Peng*[5], *Ziyue Zhu*[1], *Sadisha Nanayakkara*[6], *Veaceslav Coropceanu*[6], *Dylan G. Choi*[1], *Steven Xiao*[7], *Ahra Yi*[1,8], *Hyo Jung Kim*[8], *Jean-Luc Bredas*[6], *Harald Ade*[5], *G. N. Manjunatha Reddy*[4*], *Seth R. Marder*[3*], *John R. Reynolds*[2*], *Thuc-Quyen Nguyen*[1*]

[1] Center for Polymers and Organic Solids, Department of Chemistry and Biochemistry, University of California at Santa Barbara, Santa Barbara, CA, 93106, USA

[2] School of Chemistry and Biochemistry, School of Materials Science and Engineering, Center for Organic Photonics and Electronics, Georgia Tech Polymer Network, Georgia Institute of Technology, Atlanta, Georgia 30332, United States

[3] University of Colorado Boulder, Renewable and Sustainable Energy Institute, Boulder, CO 80303, USA

[4] University of Lille, CNRS, Centrale Lille Institut, Univ. Artois, UMR 8181, Unité de Catalyse et Chimie du Solide, F-59000, Lille, France

[5] Department of Physics and Organic and Carbon Electronics Laboratories (ORaCEL), North Carolina State University, Raleigh, NC 27695, USA

[6] Department of Chemistry and Biochemistry, The University of Arizona, Tucson, AZ, 85721-0088, USA

[7] 1-Material Inc, 2290 Chemin St-Francois, Dorval, Quebec, H9P 1K2, Canada

[8] Department of Organic Material Science and Engineering, School of Chemical Engineering, Pusan National University, Busan 46241, Republic of Korea

*Corresponding Author Emails: quyen@chem.ucsb.edu, reynolds@chemistry.gatech.edu, sema1789@colorado.edu, gnm.reddy@univ-lille.fr

Table of contents

1. Material synthesis. 4
   1.1. PM7-Dx polymer series 4
   1.2. PTI04 acceptor 16
2. Computational methodology 26
3. Solubility assessment and interaction parameters 26
   3.1. Hansen solubility parameters (HSP) 26
   3.2. Molecule–Solvent Interaction Parameter, χ 27
4. Fabrication and characterization of OPV devices 28
   4.1. Recent green solvent processing OPVs 28
   4.2. Device fabrication 28
   4.3. Differential Pulse Voltammetry (DPV) Measurements 29
5. Morphology characterization 30
   5.1. Topographic Characterization by Atomic Force Microscopy (AFM) 30
   5.2. Grazing-Incidence Wide-Angle X-ray Scattering (GIWAXS) 30
   5.3. Resonance Soft X-ray Scattering (RSoXS) 34
   5.4. X-ray photoelectron spectroscopy (XPS) 34
   5.5. Contact Angle Measurement (CAM) 35
   5.6. Flory–Huggins interaction parameter 36
   5.7. Solid-state (ss)NMR spectroscopy 36
      5.7.1. Analysis of 1D ^{1}H MAS NMR spectra of neat compounds and blends 37
      5.7.2. Analysis of 1D ^{1}H→^{13}C CP-MAS NMR spectra of neat compounds and blends 38
      5.7.3. Analysis of 2D ^{1}H-^{13}C and ^{19}F-^{19}F correlation spectra of neat compounds and blends 40
      5.7.4. Analysis of 2D ^{1}H-^{1}H DQ-SQ correlation of neat compounds and blends 42
6. References 46

1. Material synthesis.

1.1. PM7-Dx polymer series

All starting materials were purchased from a commercial supplier and were used without further purification. Bis stannyl monomer, compound 5, was purchased from SunaTech. Synthesis information of other intermediate molecules and the dibromo quaterthiophene monomers are presented in the following.

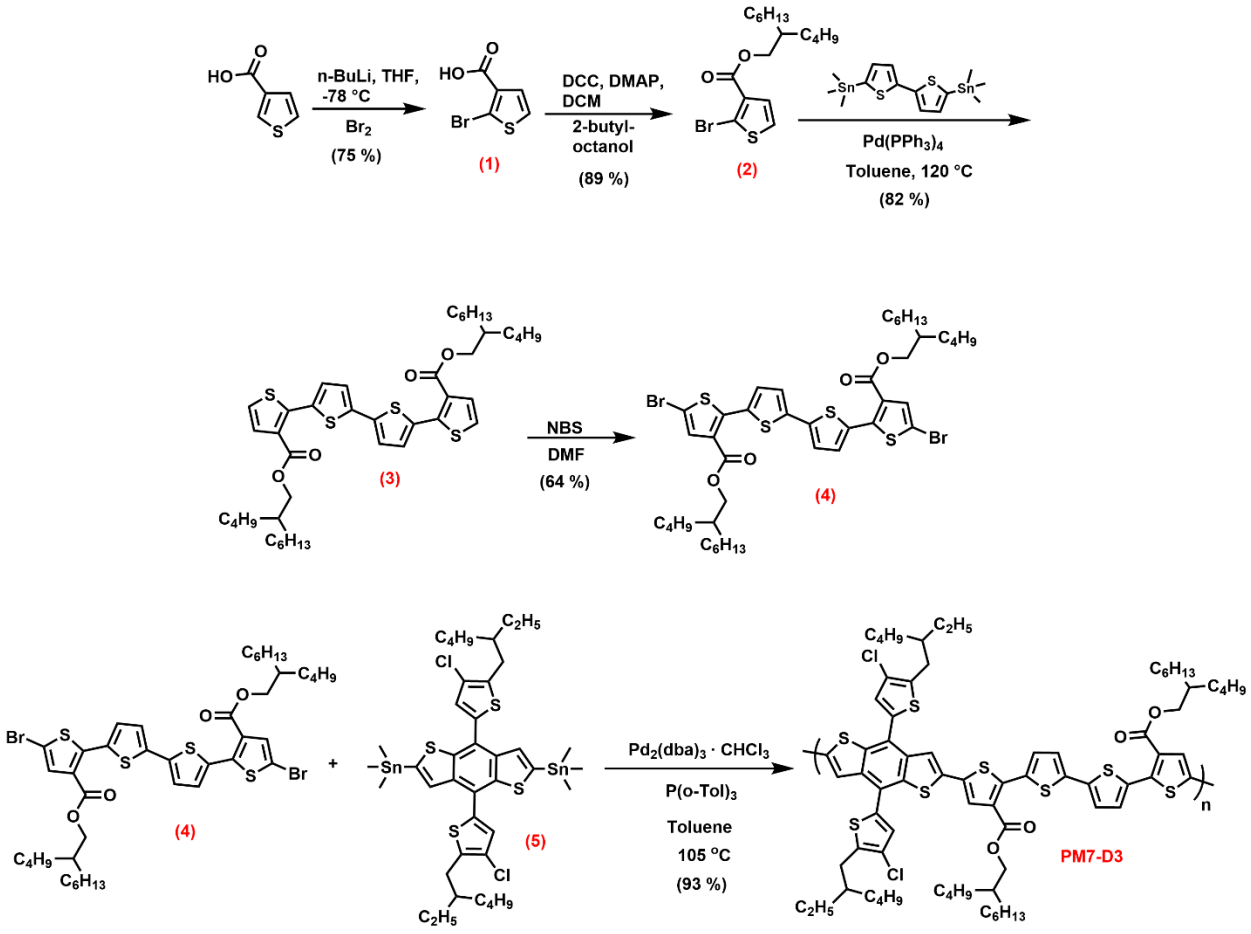

Scheme S1. Synthetic procedures of PM7-D3 and the different precursors and intermediate. Product yields are presented in the parentheses under the arrows.

Synthesis of 2-bromothiophene-3-carboxylic acid (1): Similar to a reported procedure (10.1039/D0TC03096A), 3-thiophenecarboxylic acid (5 g, 39.0 mmol) was added to a dry 250 mL round bottom flask equipped with a stir bar. After transferring the flask to the glovebox, 100 mL of dry THF was added and placed under a constant flow of argon upon removal from the glove box. The reaction vessel was chilled to -78 °C and 2 equivalents of 2.5 M n-butyllithium in hexanes (31.2 mL, 78 mmol) were added dropwise over 30 minutes. The reaction mixture was allowed to react for 3 hours at -78 °C followed by the dropwise addition of liquid bromine (2.1 mL, 40.7 mmol) at -78 °C. The mixture was then allowed to slowly warm up to room temperature while mixing over 16 hours. A small amount of HCl (2 mL of 1 M) was added to the reaction mixture turning the mixture into a clear solution. The solvent was removed under reduced pressure followed by the addition of ethyl acetate which was added to a separatory funnel and extracted with 1 M HCl twice. The organic layers were combined, dried over Na_2SO_4 and filtered. The organic solvent was removed under reduced pressure to produce an impure white powder which was recrystallized using a water/ethanol 4:1 mixture to produce white crystals (6.1 g, 75%).[1] ^{1}H NMR (500 MHz, C_2D_6OS): δ (ppm) 13.10 (s, 1H), 7.62 (d, J = 5.7 Hz, 1H), 7.32 (d, J = 5.8 Hz, 1H). NMR chemical shifts are consistent with a previous report.[1]

Synthesis of 2-butyloctyl 2-bromothiophene-3-carboxylate (2): Similar to reported procedures (10.1039/C9TA04237G, 10.1021/acs.chemmater.9b04971), 100 mL of dry dichloromethane (DCM) and 2-bromothiophene-3-carboxylic acid (1) (3 g, 14.5 mmol) were added to a dry 250 mL round bottom flask equipped with a stir bar. Then, 512 mg (4.2 mmol, 0.29 equiv.) of 4-dimethylaminopyridine (DMAP) was added followed by the addition of 1.25 equivalents of N,N'-dicyclohexylcarbodiimide (DCC) (3.75 g, 18.1 mmol). Then 1.1 equivalents of 2-butyl-1-octanol (2.97 g, 15.9 mmol) was added into the flask and the reaction mixture was left to stir overnight (16 hours) at room temperature. The solvent was removed under reduced pressure via rotary evaporation and the remaining contents were purified using silica gel column chromatography with 2:1 ratio of hexane:dichloromethane as mobile phase to afford a colorless oil (4.9 g, 89%). ^{1}H NMR (500 MHz, $CDCl_3$), δ(ppm): 7.36 (d, J = 5.8 Hz, 1H), 7.21 (d, J = 5.8 Hz, 1H), 4.20 (d, J = 5.5 Hz, 2H), 1.77-1.71 (m, 1H), 1.41-1.26 (m, 16H), 0.91-0.88 (m, 6H). ^{13}C{^{1}H} NMR (126 MHz, $CDCl_3$), δ (ppm):162.59, 131.87, 129.91, 126.18, 119.83, 68.09, 37.73, 32.21, 31.76, 31.44, 30.01, 29.35, 27.10, 23.38, 23.04, 14.49, 14.46. All NMR spectra are consistent with a previous report.[2]

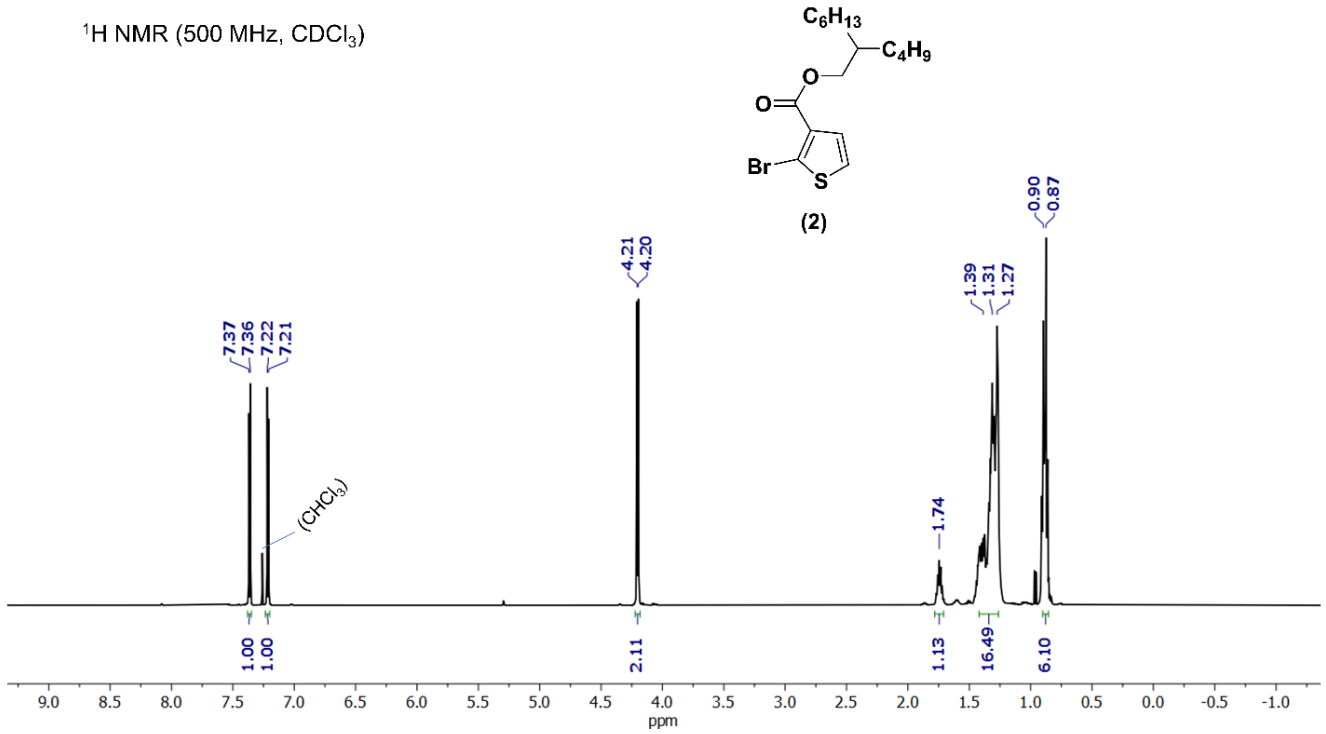

Figure S1. ^{1}H NMR of 2-butyloctyl 2-bromothiophene-3-carboxylate (2).

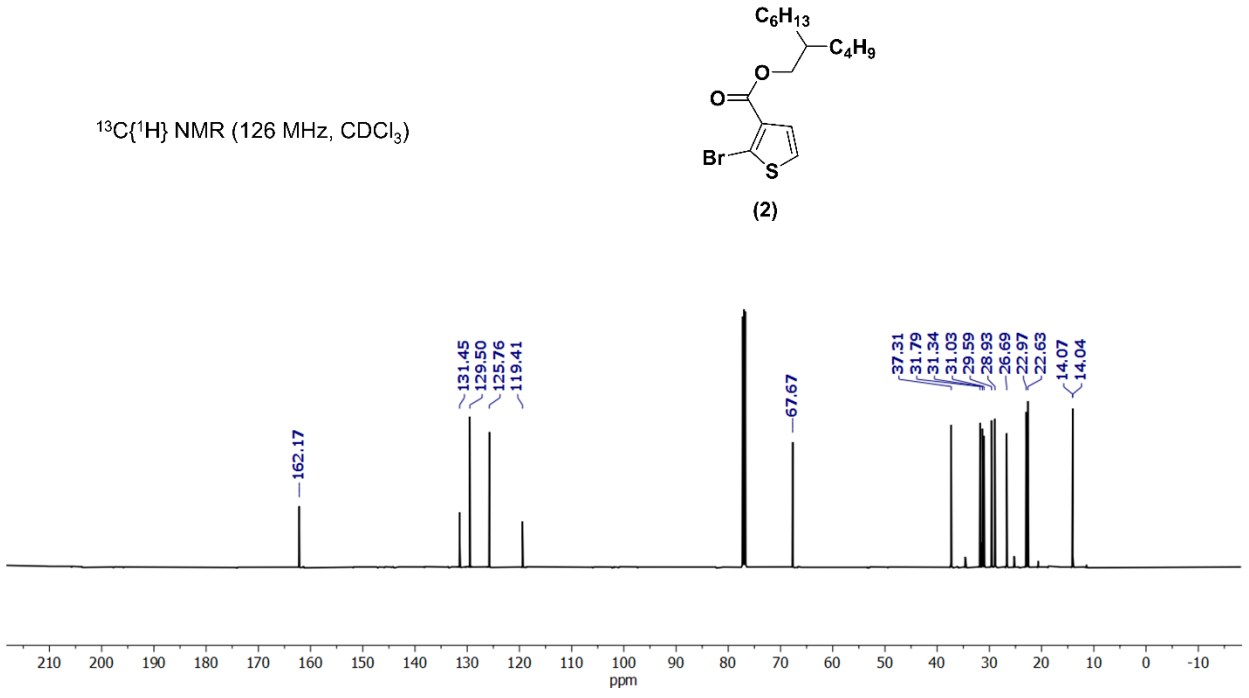

Figure S2. ^{13}C{^{1}H} NMR of 2-butyloctyl 2-bromothiophene-3-carboxylate (2).

Synthesis of bis(2-butyloctyl) [2,2':5',2'':5'',2'''-quaterthiophene]-3,3'''-dicarboxylate (3): A dry 150 mL round bottom flask equipped with a stir bar, 5,5'-bis(trimethylstannyl)-2,2'-bithiophene (2 g, 4.07 mmol), and compound 2 (3.51 g, 9.35 mmol) was transferred into a glove box. Then, tetrakis(triphenylphosphine)palladium(0) (235 mg, 0.20 mmol) was added to the flask followed by 30 mL of dry toluene. The reaction flask was removed from the glove box and heated to 120 °C and stirred for 18 hours. The solvent was removed under reduced pressure and the remaining mixture was purified using silica gel chromatography using hexane:DCM (5:2) as the eluent to produce a orange oil (2.51 g, 82%).^{1}H NMR (300 MHz, $CDCl_3$), δ(ppm): 7.48 (d, *J* = 4 Hz, 2H), 7.38 (d, *J* = 3 Hz, 2 H), 7.20 (d, *J* = 4 Hz, 2H), 7.16 (d, J = 3 Hz, 2H), 4.16 (d, *J* = 4 Hz, 4H), 1.73-1.66 (m, 2H), 1.34-1.22 (m, 32H), 0.90-0.83 (m, 12H); ^{13}C{^{1}H} NMR (126 MHz, $CDCl_3$), δ (ppm): 163.32, 142.82, 139.04, 133.25, 130.62, 130.10, 128.03, 124.03, 123.87, 67.70, 37.42, 31.91, 31.41, 31.09, 29.72, 29.03, 26.79, 23.08, 22.74, 14.18, 14.15. HR-MS (APCI) m/z for $C_{42}H_{58}O_4S_4$ theoretical (M+H): 755.3290, found (M+H): 755.3279.

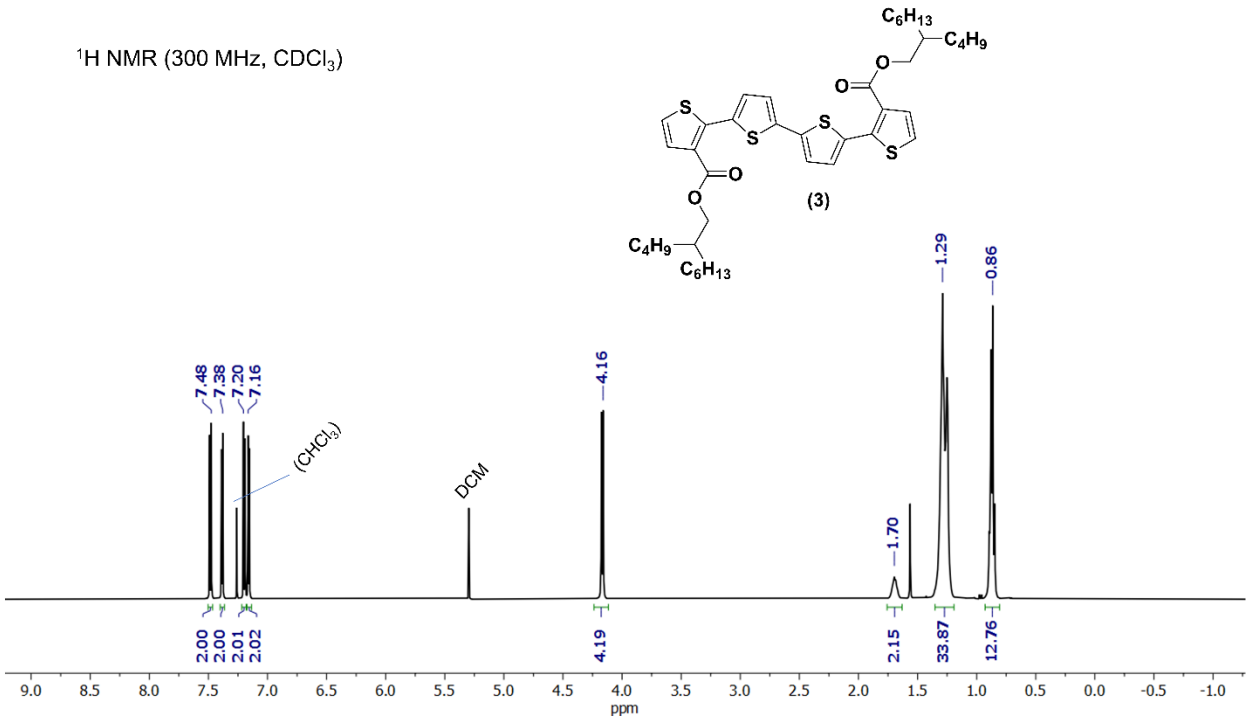

Figure S3. ^{1}H NMR of bis(2-butyloctyl) [2,2':5',2":5",2"'-quaterthiophene]-3,3"'-dicarboxylate (3).

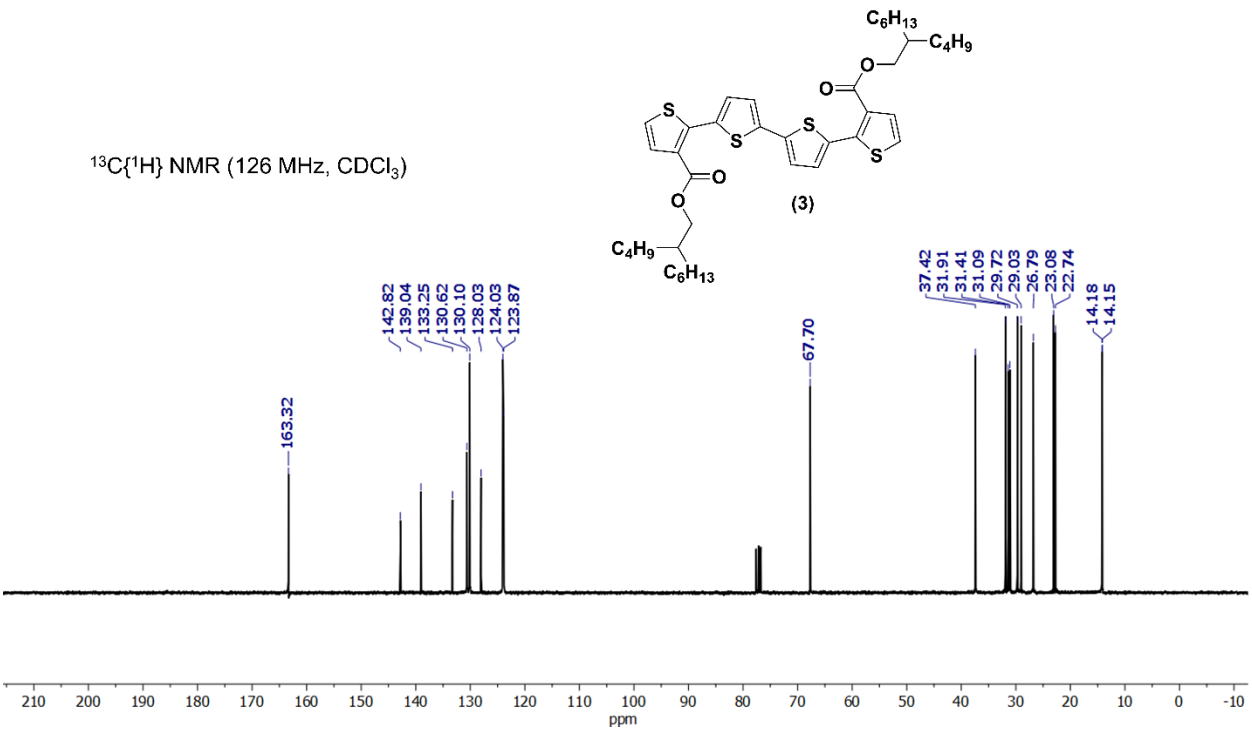

Figure S4. $^{13}C\{^{1}H\}$ NMR of bis(2-butyloctyl) [2,2':5',2":5",2"'-quaterthiophene]-3,3"'-dicarboxylate (3).

Synthesis of bis(2-butyloctyl) 5,5'''-dibromo-[2,2':5',2'':5'',2'''-quaterthiophene]-3,3'''-dicarboxylate (4): To a 150 mL round bottom flask was added a stir bar, compound 3 (2 g, 2.65 mmol) and 70 mL of DMF. Then 2.7 equivalents of NBS (1.27 g, 7.13 mmol) was added to the solution in small portions at 0 °C. The reaction was sealed, protected from light and stirred for 16 hours. Subsequently, the solvent was removed under reduced pressure followed by an extraction using DCM and water. The organic layer was dried over Na_2SO_4, filtered and concentrated under reduced pressure. The crude product was purified using silica gel chromatography using hexane:DCM (4:1) as the eluent to produce an orange solid (1.55 g, 64%).^{1}H NMR (300 MHz, $CDCl_3$), δ(ppm): 7.42 (s, 2H), 7.33 (d, *J* = 3 Hz 2H), 7.14 (d, *J* = 3 Hz 2H), 4.16 (d, *J* = 4 Hz, 4H), 1.72-1.64 (m, 2H), 1.34-1.20 (m, 32H), 0.92-0.83 (m, 12H); $^{13}C\{^{1}H\}$ NMR (126 MHz, $CDCl_3$), δ (ppm):162.26, 144.14, 139.48, 132.89, 132.26, 130.55, 128.33, 124.31, 110.82, 68.11, 37.44,

31.97, 31.43, 31.12, 29.75, 29.09, 26.84, 23.13, 22.80, 14.25, 14.21. HR-MS (APCI) m/z for $C_{42}H_{56}Br_2O_4S_4$ theoretical (M+H): 911.1501, found (M+H): 911.1485.

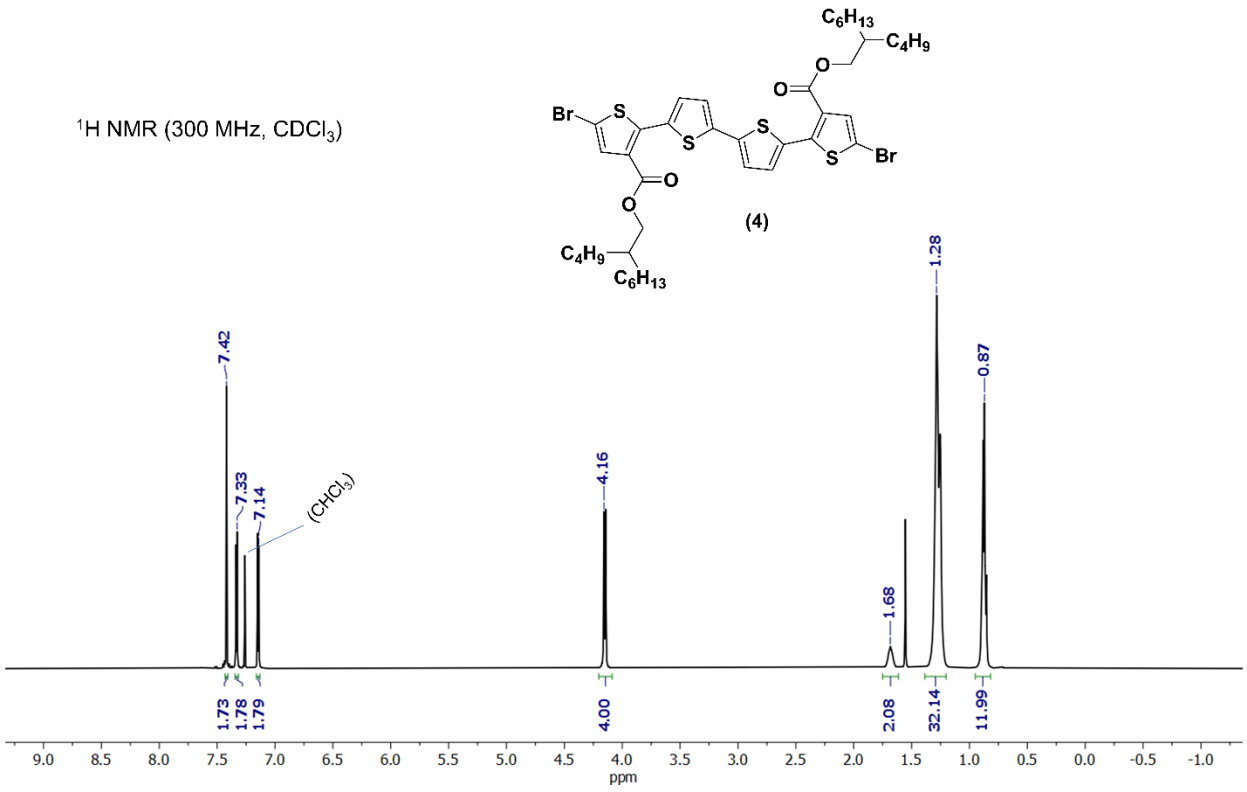

Figure S5. ^{1}H NMR of bis(2-butyloctyl) 5,5'''-dibromo-[2,2':5',2'':5'',2'''-quaterthiophene]-3,3'''-dicarboxylate (4).

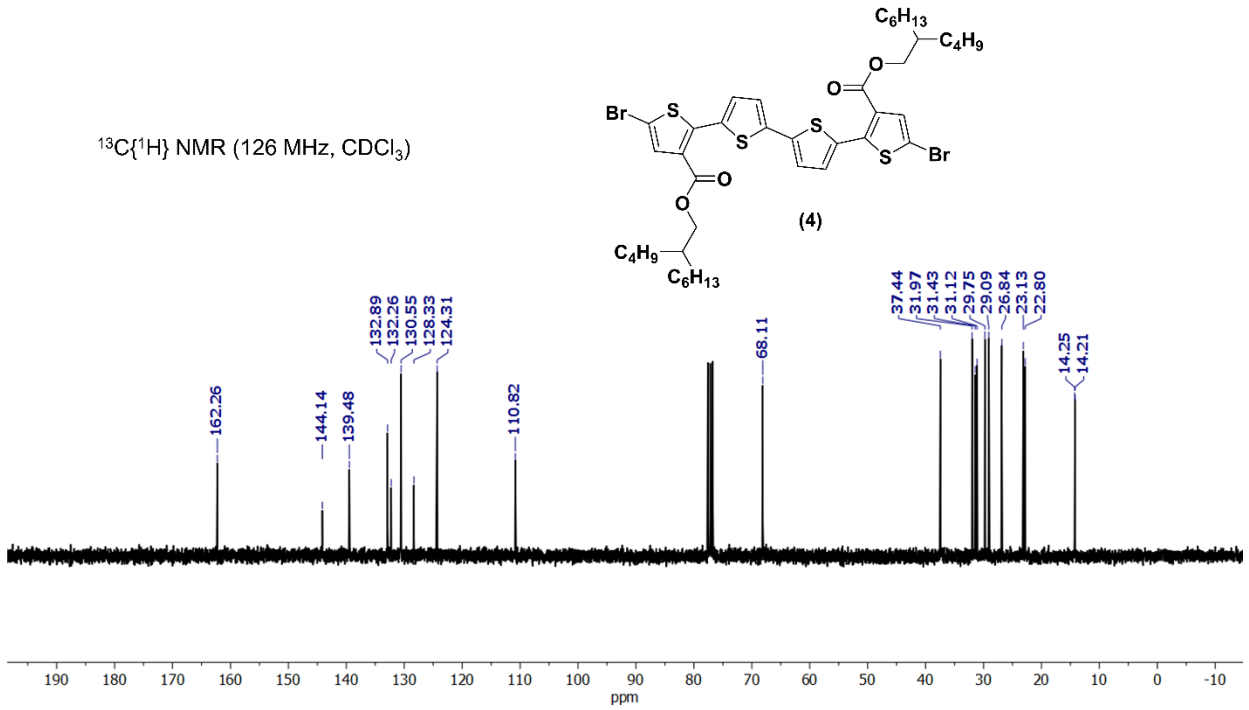

Figure S6. $^{13}C\{^{1}H\}$ NMR of bis(2-butyloctyl) 5,5'''-dibromo-[2,2':5',2'':5'',2'''-quaterthiophene]-3,3'''-dicarboxylate (4).

Polymerization Procedure: (4,8-Bis(4-chloro-5-(2-ethylhexyl)thiophen-2-yl)benzo[1,2-b:4,5-b']dithiophene-2,6-diyl)bis(tri -methylstannane) (compound 5, 248 mg, 0.255 mmol, 1 equiv.) and the complementary co-monomer, di-bromo di-ester quaterthiophene (compound 4, 233 mg, 0.255 mmol, 1 equiv.) were added to a dry 50 mL round bottom flask equipped with a magnetic stir bar. The round bottom was transferred into a glove box where toluene (10 mL), $Pd_2(dba)_3.CHCl_3$ (7.9 mg, 0.03 equiv.), and $P(o\text{-}tol)_3$ (9.3 mg, 0.12 equiv.) were added to the flask. The vessel was capped and removed from the glove box and put under the constant flow of argon. Next, the reaction vessel was heated to 105 °C and allowed to react for 24 hours. The polymerization was then cooled to 90 °C and exposed to air to add an excess amount of Pd scavenger diethylammonium diethyldithiocarbamate and 10 mL of chlorobenzene. The mixture was stirred for 1 hour before it was precipitated into 250 mL of methanol. The impure polymer was filtered through a cellulose extraction thimble and subjected to successive Soxhlet extractions with methanol, acetone,

hexanes, and finally recovered from chloroform. The chloroform solution of the purified product was concentrated under reduced pressure and precipitated into methanol. Finally, the pure polymer powder was collected via vacuum filtration and dried under vacuum for 24 hours.

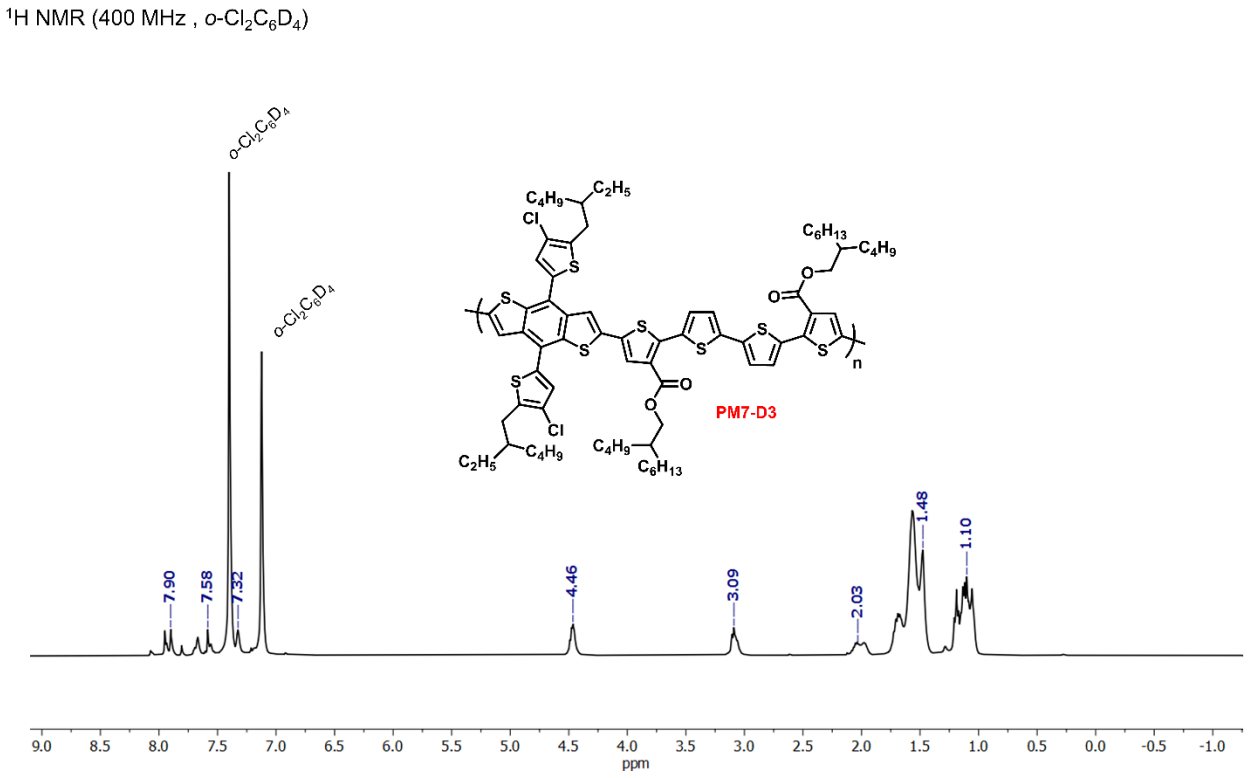

Figure S7. ^{1}H NMR spectra of PM7-D3 in o-dichlorobenzene-D4 at 110 °C. δ (ppm): 8.08-7.78 (m, 4H), 7.71-7.53 (m, 4H), 7.32 (s, 2H), 4.46 (m, 4H), 3.09 (m, 4H), 2.03 (m, 4H), 1.78-1.41 (m, 48H), 1.25-1.00 (m, 24H).

Synthesis of PM7-D5: Synthesis scheme for PM7-D5 is summarized in the below scheme. Details of synthesis procedure for intermediate molecules from 3-thiophenecarboxylic to dibromo diester quaterthiophene isomer (compound 11) where ester groups are attached to other positions of inner thiophene are presented in a recent article.[3]

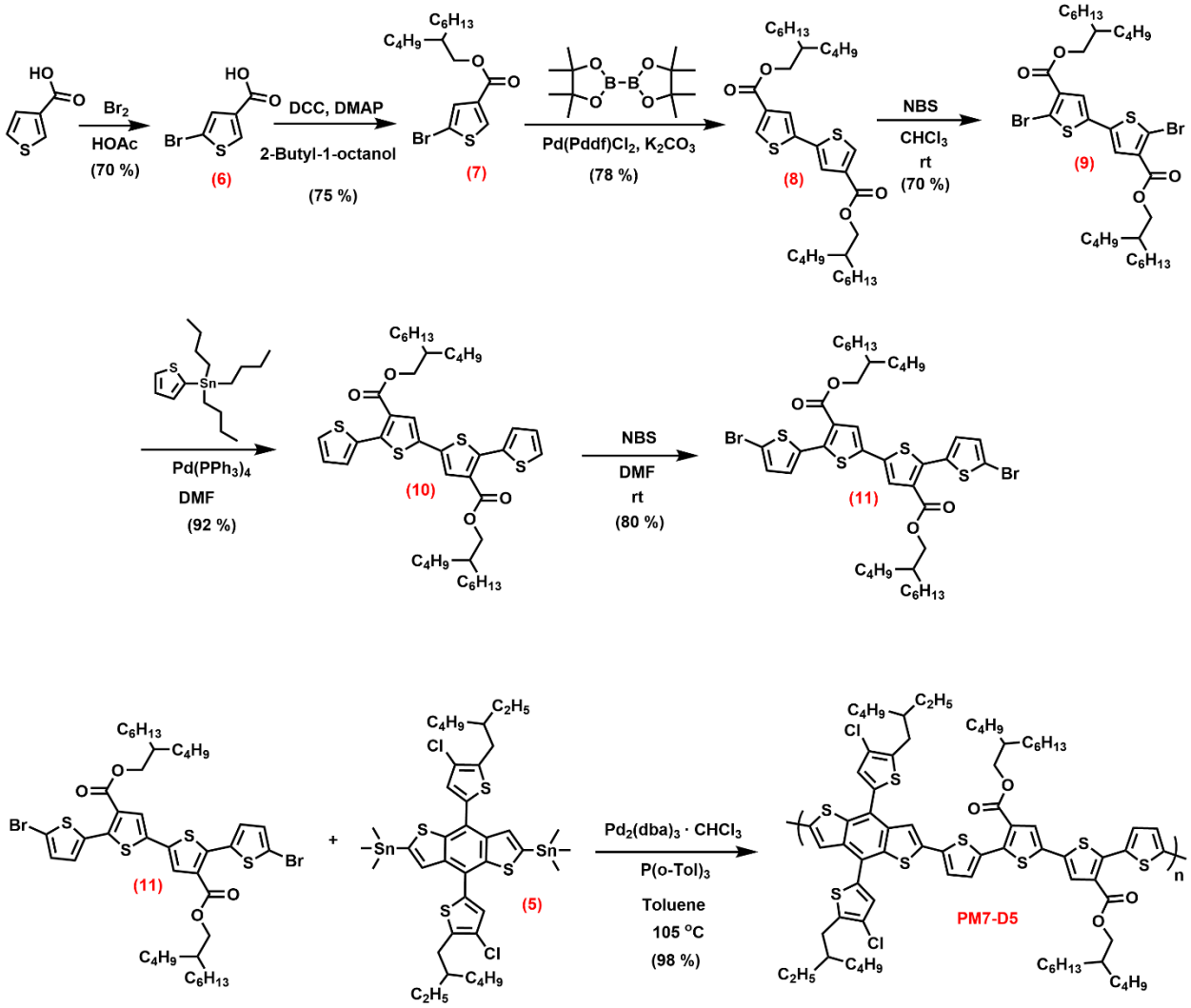

Scheme S2. Synthetic procedures of PM7-D5 and the different precursors and intermediate molecules. Product yields are presented in the parentheses.

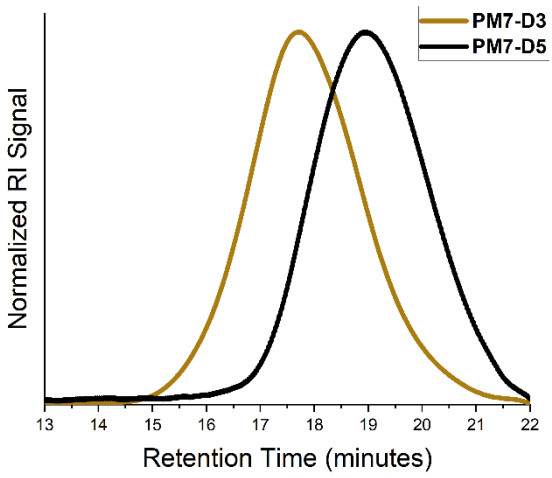

Figure S8. High temperature (140 °C) GPC trace of PM7-D3 (Mn: 64.6 kg/mol, Mw: 148.6 kg/mol, Đ: 2.30) PM7-D5 (Mn: 26.1 kg/mol, Mw: 54.5 kg/mol, Đ: 2.09) and in 1,2,4-trichlorobenzene. (vs polystyrene).

Table S1. Purity assessment using elemental analysis for PM7-D3 and PM7-D5 polymers with the same elemental content.

Studied Element	Theoretical %	Experimental % For PM7-D3	Experimental % For PM7-D5
C	65.25	65.49	65.53
H	6.77	6.88	6.80
S	18.33	18.20	18.35

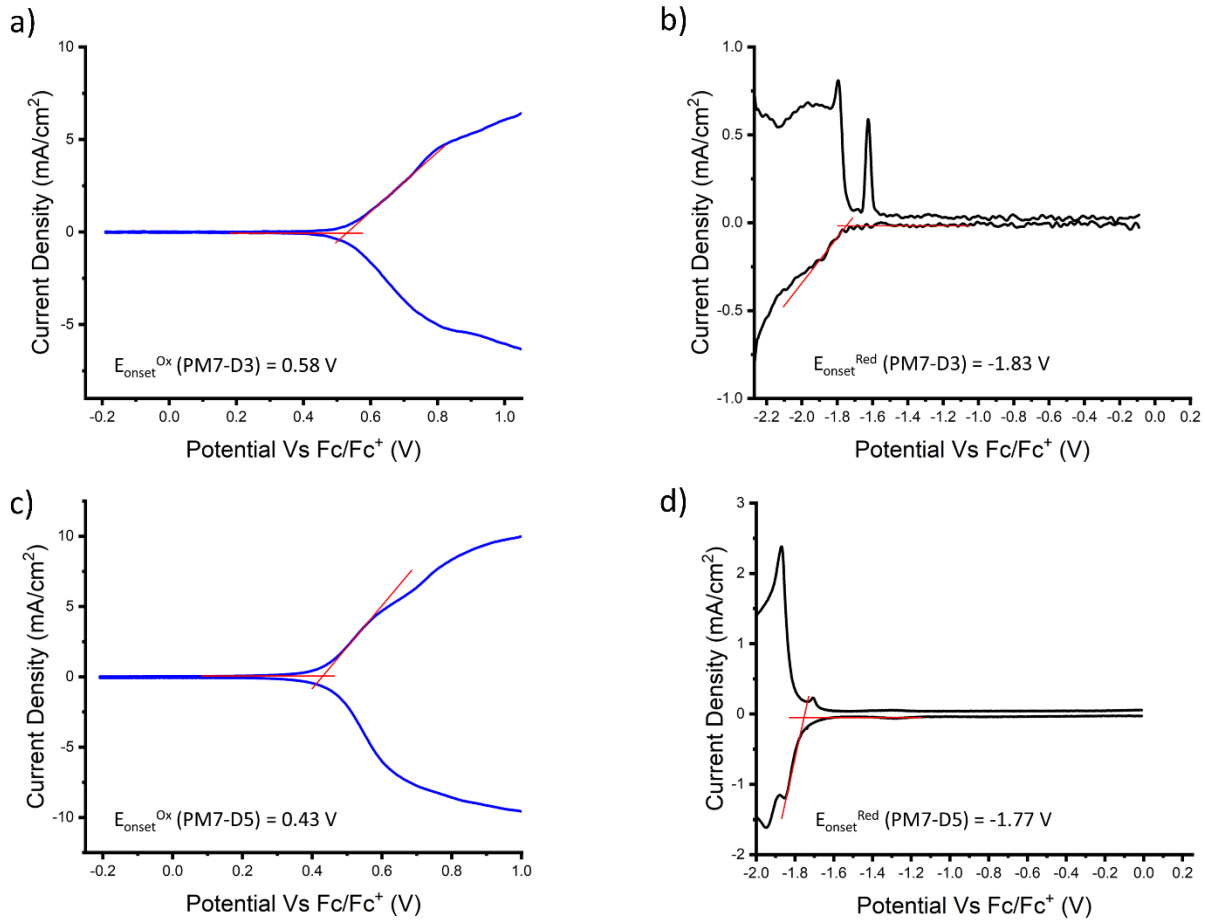

Figure S9. Dynamic pulse voltammetry (DPV) results of oxidative (a and c) and reductive (b and d) scans versus Fc/Fc^+ for PM7-D3 and PM7-D5 to respectively find ionization energy and electron affinity (ionization energy and electron affinity values are calculated by assuming saturated calomel electrode (SCE) versus vacuum with respect to Fc/Fc^+ to be 5.12 eV).

Synthetic characterizations:^{1}H NMR and ^{13}C NMR spectra for all monomers and molecular precursors were acquired on a Bruker Avance IIIHD 500 MHz or Bruker Avance IIIHD 700 MHz instruments using $CDCl_3$ as solvent; the residual $CHCl_3$ peak was used as a reference for all reported chemical shifts (^{1}H: δ = 7.26 ppm, ^{13}C: δ = 77.16 ppm). ^{1}H NMR for the polymer was acquired on a Bruker Avance IIIHD 400 MHz using *o*-dichlorobenzene-D4 as the solvent at

110 °C; the residual solvent peak was used as a reference for the polymer chemical shifts (^{1}H: δ = 6.93 ppm, and δ = 7.20 ppm). Mass spectroscopy of small molecules were obtained by direct infusion atmospheric pressure chemical ionization (APCI) in positive mode using a Thermo Scientific Orbitrap ID-X Tribrid mass spectrometer. Gel permeation chromatography (GPC) was performed using a Tosoh EcoSEC high temperature GPC instrument with RI detector to determine the number-average molecular weight (M_n), weight average molecular weight (M_w) and dispersity (*Đ*) for all polymers. Experiments were run using 1,2,4-trichlorobenzene (TCB) as eluent at 140 °C at a flow rate of 1 mL/min on two 7.8 mm x 30 cm, 13 μm TSK-Gel GMHHR-H(S) HT2 columns in series. The instrument was calibrated using polystyrene standards (1,390-1,214,000 g/mol) and the data were analyzed using 8321GPC-WS analysis software. The GPC samples were prepared by dissolving the polymers in TCB at a 1 mg/mL concentration and stirred at 120 °C for at least 3 hours before filtering through a 0.45 mm PTFE filter. Elemental analyses were conducted by Atlantic Microlab Inc.

1.2. PTI04 acceptor

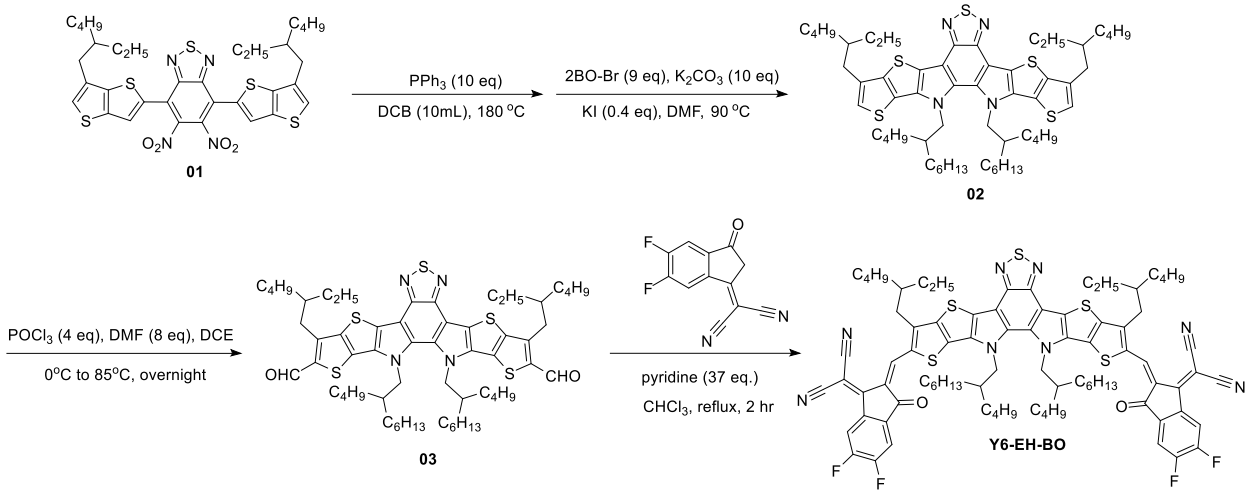

Scheme S3. Synthetic procedure of **PTI04**

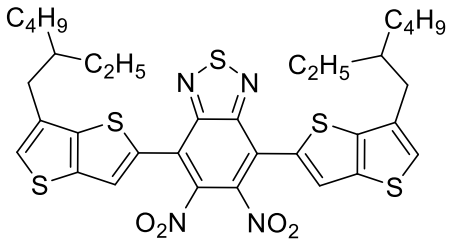

4,7-Bis(6-(2-ethylhexyl)thieno[3,2-b]thiophen-2-yl)-5,6-dinitrobenzo[c][1,2,5]thiadiazole (01): Compound **01** was synthesized by following the literature-reported procedure.[4]

^{1}H NMR (500 MHz, $CDCl_3$) δ 7.75 – 7.71 (m, 2H), 7.20 – 7.16 (m, 2H), 2.73 (d, *J* = 7.1 Hz, 4H), 1.85 – 1.72 (m, 2H), 1.59 – 1.55 (m, 2H), 1.42 – 1.31 (m, 14H), 0.98 – 0.88 (m, 12H). HRMS (MALDI) m/z $[M]^+$ calcd. for $C_{34}H_{38}N_4O_4S_5$ 726.1491; found 726.1502.

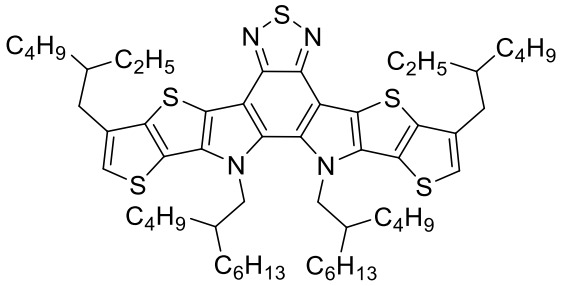

3,9-Bis(2-ethylhexyl)-12,13-bis(2-butyloctyl)-12,13-dihydro-[1,2,5]thiadiazolo[3,4-e]thieno [2'',3'':4',5']thieno[2',3':4,5]pyrrolo[3,2- g]thieno[2',3':4,5]thieno[3,2-b]indole (02): Compound **01** (1.38 mmol) and triphenylphosphine (13.8 mmol) was dissolved in *o*-dichlorobenzene (10 mL) under nitrogen. After being reflux at 180 ^{o}C overnight, *o*-dichlorobenzene was distilled out of the reaction. Then, the excess triphenylphosphine was eliminated by flash column chromatography on silica gel using chloroform as eluent. The red residue was mixed with K_2CO_3 (13.8 mmol), KI (0.55 mmol) and 2-butyloctyl bromide (12.4 mmol) in a two neck-round bottom flask. The mixture was deoxygenated with nitrogen for 15 min. Anhydrous DMF (40 mL) was added to the mixture, and the mixture was heated up to 90 ^{o}C overnight. The cooled down mixture was filtered through Celite and washed with DCM. The organic layers were combined, concentrated in vacuo, and purified with column chromatography on silica gel using DCM/hexane (1/4, v/v) as the eluent to give an orange solid product (85% yield).

^{1}H NMR (400 MHz, $CDCl_3$) δ 7.02 (s, 2H), 4.61 (d, *J* = 7.8 Hz, 4H), 4.05 (d, *J* = 5.9 Hz, 2H), 2.78 (m, 4H), 2.10 (s, 2H), 1.98 (s, 2H), 1.48 – 1.35 (m, 20H), 1.03 – 0.85 (m, 30H), 0.75 – 0.56 (m, 20H). HRMS (MALDI) m/z $[M]^+$ calcd. for $C_{58}H_{86}N_4S_5$ 998.5450; found 998.5478.

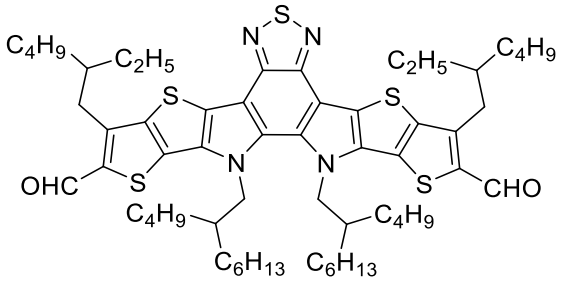

3,9-Bis(2-ethylhexyl)-12,13-bis(2-butyloctyl)-12,13-dihydro-[1,2,5]thiadiazolo[3,4-e]thieno [2'',3'':4',5']thieno[2',3':4,5]pyrrolo[3,2-g]thieno[2',3':4,5]thieno[3,2-b]indole-2,10-dicarbaldehyde (03): To a solution of dichloroethane (4 mL) with DMF (9.4 mmol) at 0 °C, $POCl_3$ (4.7 mmol) was added slowly under nitrogen. The mixture was allowed to heat up to room temperature for 20 min. Then, the solution of compound **02** (1.2 mmol) in DCE (15 mL) was transferred to the mixture at 0 °C. After being reflux at 85 °C overnight, 1M NaOH (20 mL) was added and stirred for 3 h. The mixture was extracted with DCM and water, and the organic layers were combined, concentrated in vacuo, and purified with column chromatography on silica gel using DCM/hexane (1/1, v/v) as the eluent to give an orange solid product (78% yield).

^{1}H NMR (400 MHz, $CDCl_3$) δ 10.11 (s, 2H), 4.60 (d, *J* = 7.9 Hz, 4H), 3.09 (d, *J* = 7.5 Hz, 4H), 2.01 (q, *J* = 6.6 Hz, 4H), 1.47 – 1.26 (m, 16H), 1.07 – 0.78 (m, 41H), 0.61 (ddt, *J* = 19.5, 14.3, 7.0 Hz, 15H). ^{13}C{^{1}H} NMR (101 MHz, $CDCl_3$) δ 181.97, 147.47, 146.37, 143.39, 143.37, 137.74, 136.75, 132.90, 129.51, 127.38, 112.33, 110.00, 55.22, 40.59, 40.53, 38.81, 32.91, 32.73, 31.45, 30.21, 30.17, 30.10, 30.04, 29.26, 29.25, 28.79, 27.79, 27.64, 26.12, 25.21, 25.05, 22.97, 22.68, 22.65, 22.40, 22.38, 14.06, 13.91, 13.67, 13.64, 10.85, 10.83. Anal. Calcd for $C_{60}H_{86}N_4O_2S_5$ (%): C, 68.27; H, 8.21; N, 5.31. Found (%): C, 68.53; H, 8.12; N, 5.33. HRMS (MALDI) m/z $[M]^+$ calcd. for $C_{60}H_{86}N_4O_2S_5$ 1054.5349; found 1054.5377.

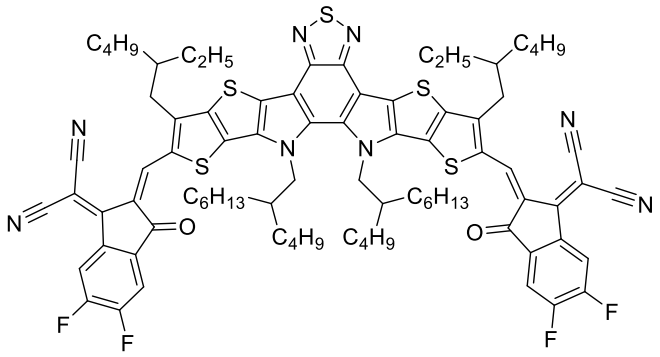

2,2'-((2Z,2'Z)-((3,9-Bis(2-ethylhexyl)-12,13-bis(2-butyloctyl)-12,13-dihydro-[1,2,5]thiadiazolo [3,4-e]thieno[2'',3'':4',5']thieno[2',3':4,5]pyrrolo[3,2-g]thieno[2',3':4,5]thieno[3,2-b]indole-2,10-diyl)bis(methaneylylidene))bis(5,6-difluoro-3-oxo-2,3-dihydro-1H-indene-2,1-diylidene)) dimalononitrile (PTI04): The solution of compound **03** (0.1 mmol) and 2-(5, 6-difluoro-3-oxo-2,3-dihydro-1H-inden-1-ylidene) malononitrile (0.6 mmol) in dry chloroform (8 mL) were slowly added pyridine (3.5 mmol) under nitrogen. The mixture was stirred at reflux for 2 h. After cooling to room temperature, the mixture was poured into methanol and filtered. The residue was purified with column chromatography on silica gel using chloroform/hexane (3/1, v/v) as the eluent to give a dark blue solid (86% yield). ^{1}H NMR (400 MHz, $CDCl_3$) δ 9.12 (s, 2H), 8.53 (dd, *J* = 10.0, 6.4 Hz, 2H), 7.66 (t, *J* = 7.5 Hz, 2H), 4.72 (d, *J* = 8.0 Hz, 4H), 3.15 (d, *J* = 7.7 Hz, 4H), 2.13 – 2.03 (m, 2H), 2.03 – 1.93 (m, 2H), 1.49 – 1.41 (m, 4H), 1.41 – 1.19 (m, 13H), 1.18 – 0.94 (m, 17H), 0.90 (t, *J* = 7.3 Hz, 16H), 0.83 (t, *J* = 6.9 Hz, 10H), 0.61 (p, *J* = 7.1 Hz, 12H). ^{13}C{^{1}H} NMR (101 MHz, $CDCl_3$) δ 159.08, 153.43, 147.49, 145.35, 137.51, 135.71, 134.15, 134.07, 130.93, 120.08, 115.09, 114.58, 113.45, 55.62, 41.43, 39.14, 34.41, 32.65, 31.54, 30.35, 29.36, 28.77, 27.77, 25.97, 23.00, 22.76, 22.43, 14.08, 13.99, 13.72, 10.96. Anal. Calcd for $C_{84}H_{90}F_4N_8O_2S_5$(%): C, 68.17; H, 6.13; N, 7.57. Found (%):C, 68.25; H, 6.25; N, 7.58. HRMS (MALDI) m/z $[M]^+$ calcd. for $C_{84}H_{90}F_4N_8O_2S_5$ 1478.5721; found 1478.5755.

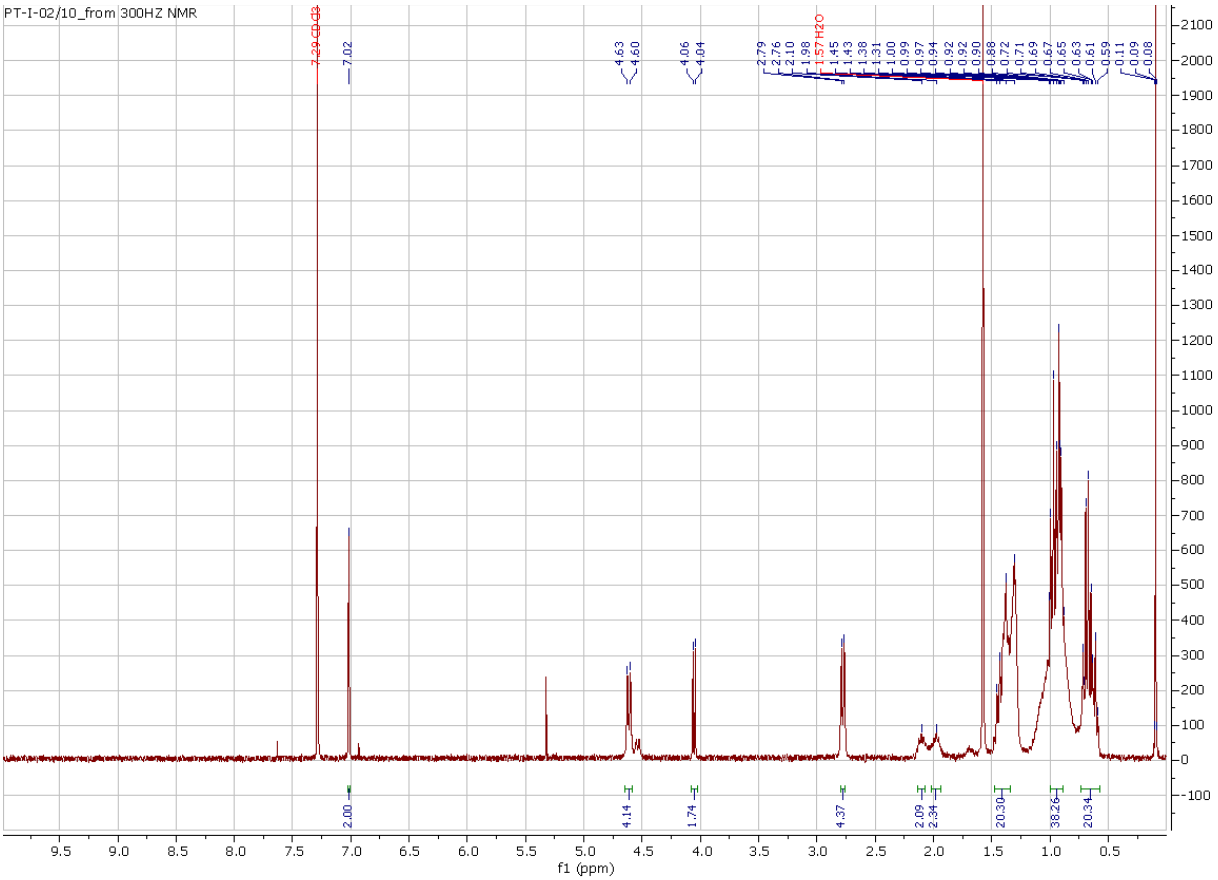

Figure S10. The ^{1}H-NMR spectra of **02**.

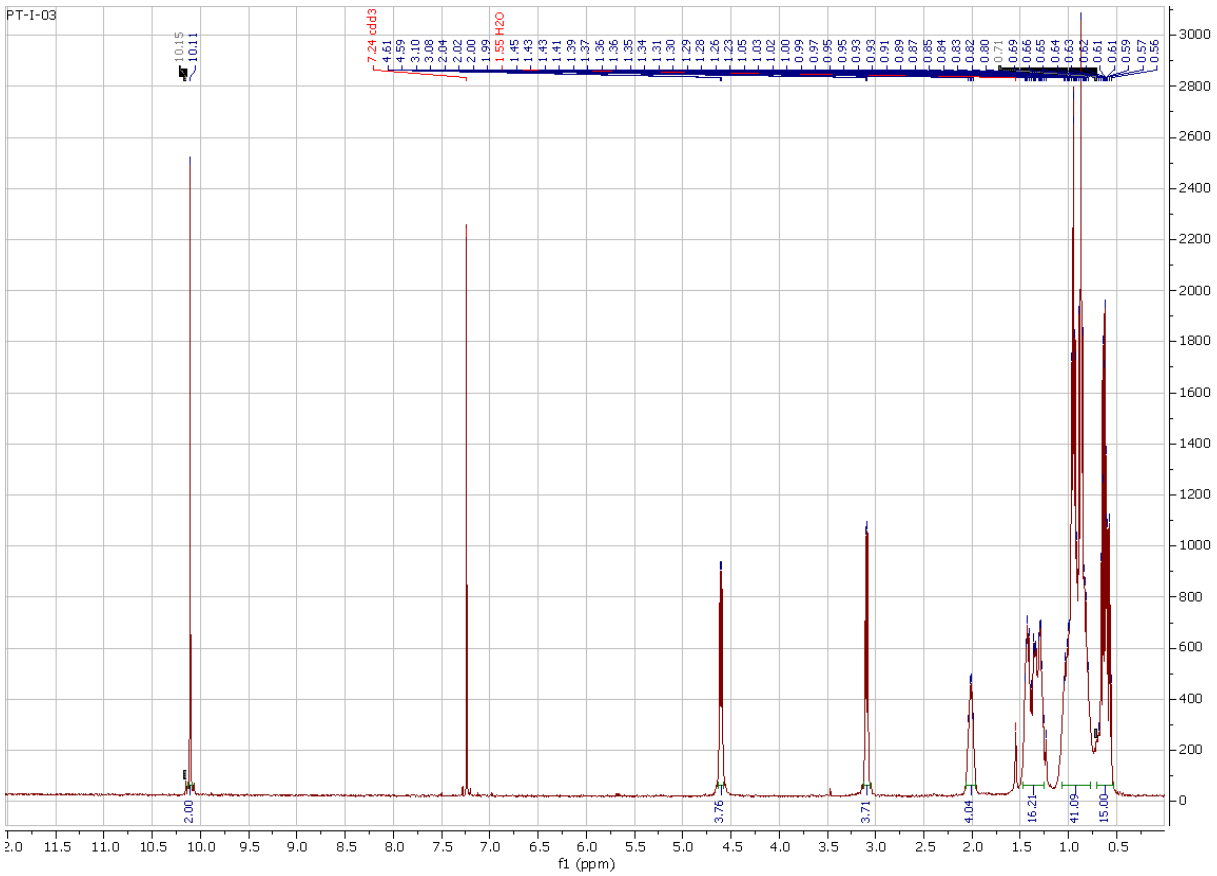

Figure S11. The ^{1}H-NMR spectra of **03**.

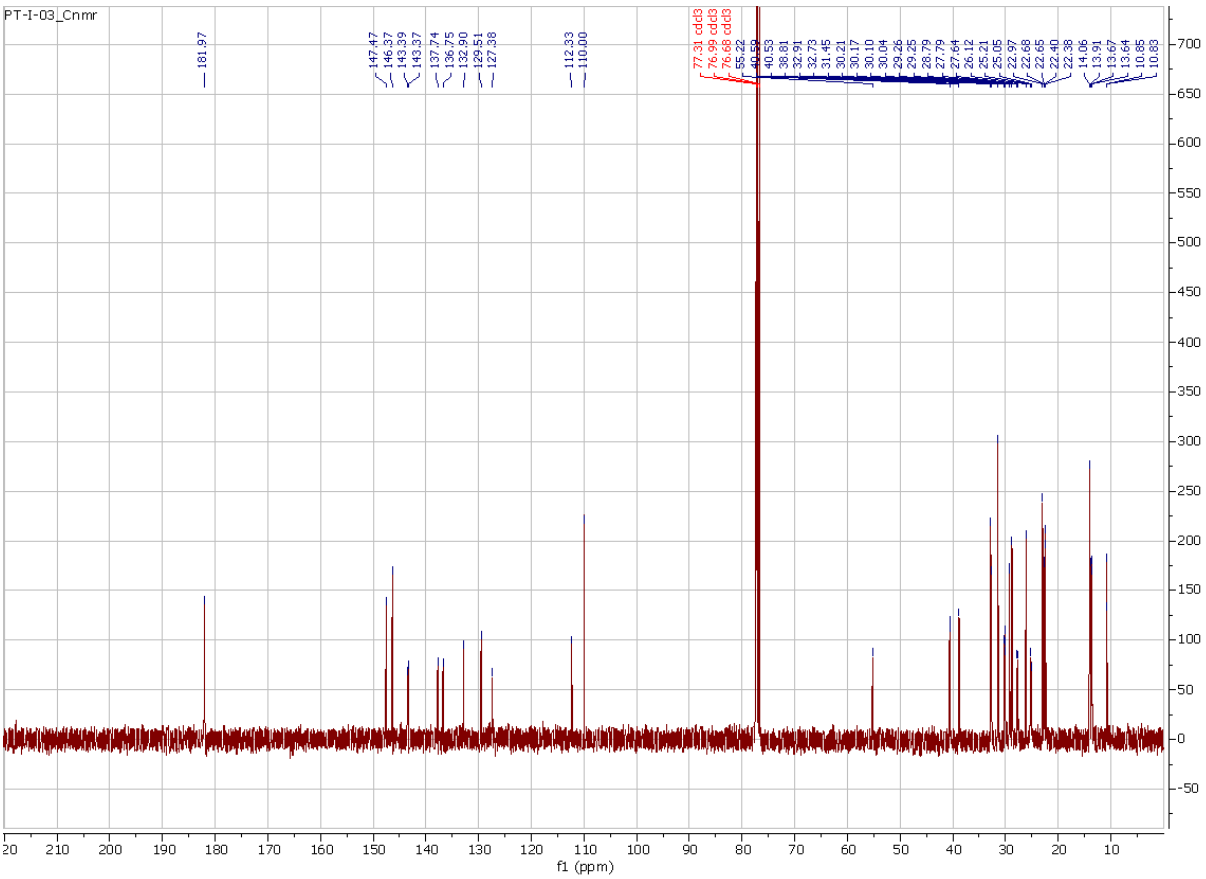

Figure S12. The ^{13}C-NMR spectra of **03**.

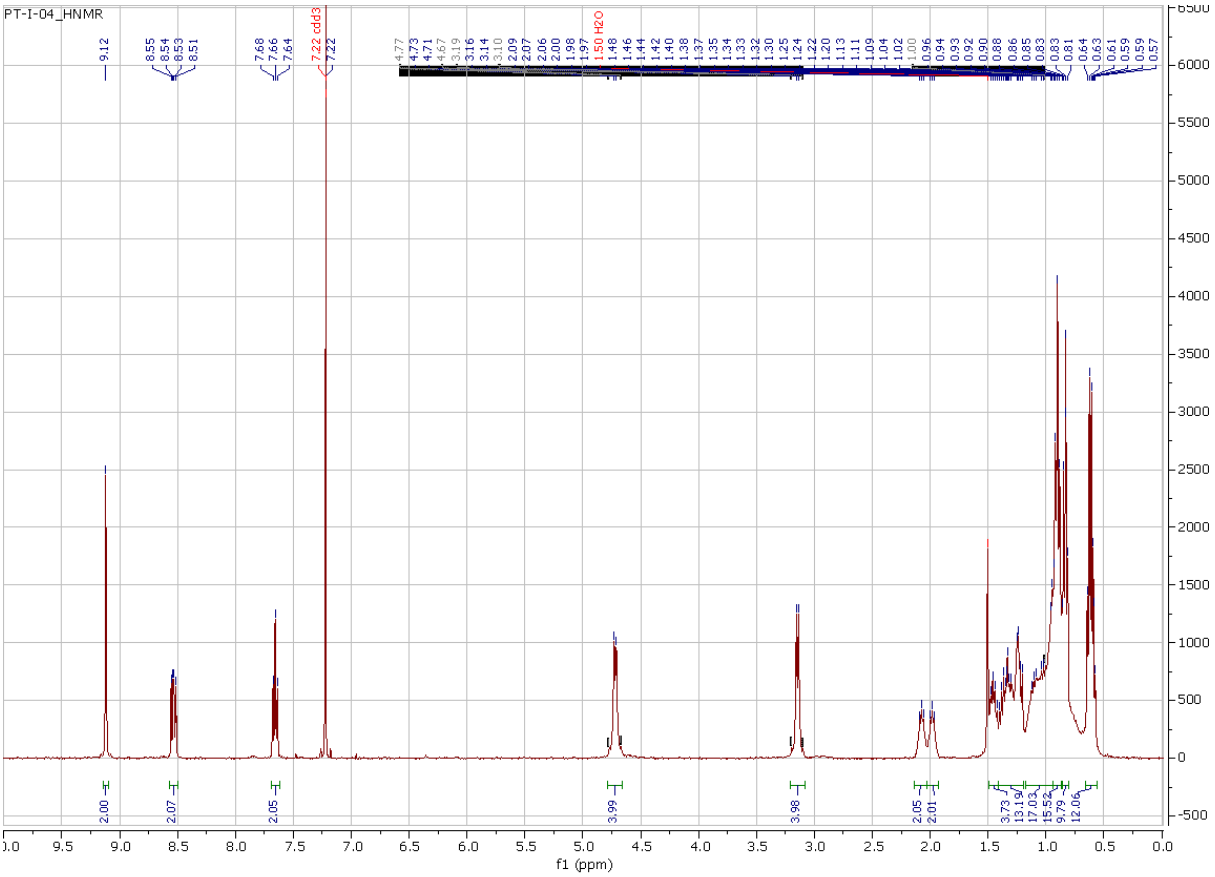

Figure S13. The ^{1}H-NMR spectra of **PTI04**.

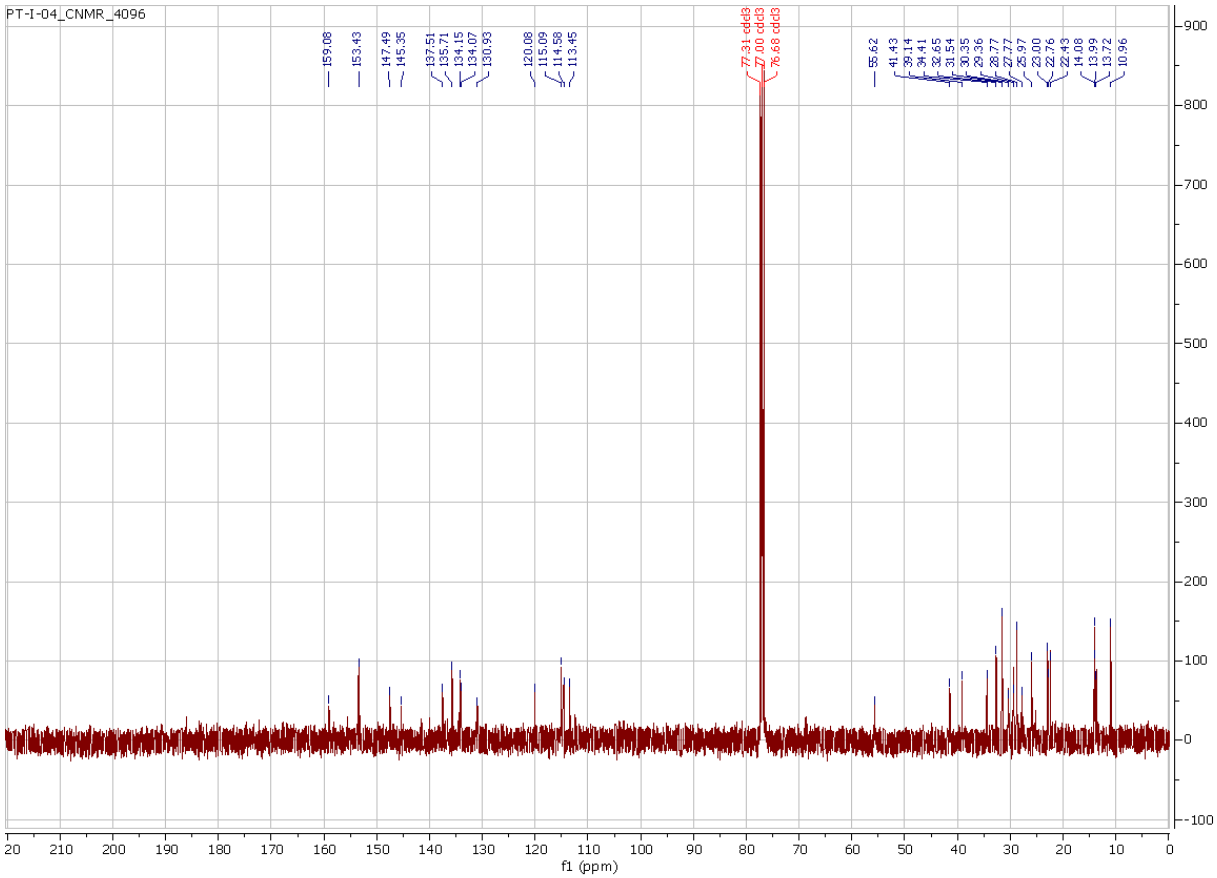

Figure S14. The ^{13}C-NMR spectra of **PTI04**.

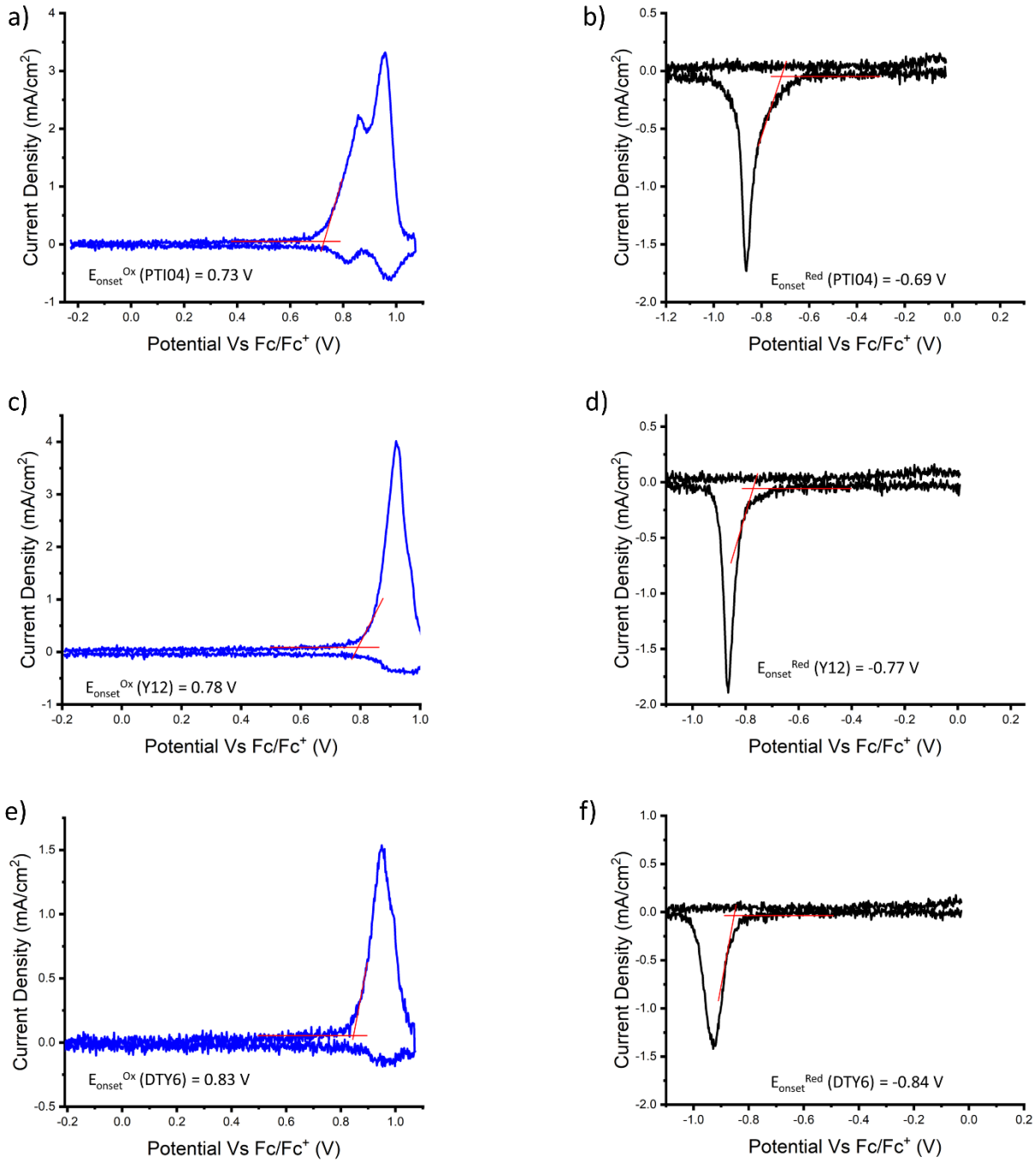

Figure S15. Dynamic pulse voltammetry (DPV) results of oxidative (a, c and e) and reductive (b, d, and d) scans versus Fc/Fc$^+$ for PTI04, Y12, and DTY6 to respectively find ionization energy and electron affinity (ionization energy and electron affinity values are calculated by assuming saturated calomel electrode (SCE) versus vacuum with respect to Fc/Fc$^+$ to be 5.12 eV).

2. Computational methodology

Isolated oligomers consisting of symmetric dimer units (two monomers and an additional quaterthiophene unit) were considered as models for the PM7-D3 and PM7-D5 polymers. Geometry optimizations were performed with the long-range corrected ωB97X-D[5] density functional and the 6-31G(d, p)[6] basis set. To prevent having the optimization stuck within a local minimum, several initial conformations were accounted for in the case of monomers, and dimers were then derived for the most stable conformations resulting from those monomer calculations. The calculations of the monomer and dimer systems considered the sidechains in their entirety. For the evaluation of the ionization potentials (IPs), range-separated parameter, ω, was optimally tuned to be 0.003 $Bohr^{-1}$ by minimizing the function $J(\omega) = (E_{HOMO} + IP)^2 + (E_{LUMO} + EA)^2$, in the framework of the polarizable continuum model[7] (PCM), considering ε = 4.0 as the dielectric constant of the medium (typical range for ε is 3~5 for π-conjugated materials). All electronic-structure calculations were carried out with the Gaussian 16 package.[8]

3. Solubility assessment and interaction parameters

3.1. Hansen solubility parameters (HSP)

To have a better understanding on why molecular designs of PM7-Dx polymer and NFAs improve their solubilities in 2-MeTHF, we employed a Hansen solubility method that partitions the Hildebrand parameter δ_T into three individual intramolecular factors: the dispersion (δ_D), polar (δ_P), and hydrogen bonding (δ_H) parameters.[9-11]

$$\delta_D = \frac{\sum F_{Di}}{V}$$

$$\delta_P = \frac{\sqrt{\sum F_{Pi}^2}}{V}$$

$$\delta_D = \sqrt{\frac{\sum E_{Hi}}{V}}$$

where V is the molar volume, F_{Di}, F_{Pi}, and E_{Hi} are the i group contributions to the whole dispersion (F_D), polar (F_P), and hydrogen bonding (F_H) components. The intramolecular factors of molecules in this study are estimated and summarized in **Table S2**.

Table S2. Intramolecular factors of donor and acceptor molecules used in this study

Chemical	δ_D	δ_P	δ_H
PM7-D3/D5	26.07	2.64	6.26
Y6	19.33	3.73	2.77
Y7	19.88	6.26	3.06
Y12	18.98	3.22	2.57
PTI04	19.27	3.73	2.77
DTY6	18.34	2.28	2.17
2-MeTHF	16.40	4.80	4.90
CF	17.80	3.10	5.70

3.2. Molecule–Solvent Interaction Parameter, χ

From the intramolecular factors of molecules and solvents, the molecule-molecule interaction parameter (χ) between them can be calculated as follows,

$$\chi = \alpha \frac{V_s}{RT}\left(\left(\delta_{Dp} - \delta_{Ds}\right)^2 + \frac{1}{4}\left(\delta_{Pp} - \delta_{Ps}\right)^2 + \frac{1}{4}\left(\delta_{Hp} - \delta_{Hs}\right)^2\right)$$

Table S3. Molecule–solvent interaction parameter, χ, between molecule in this study and 2-MeTHF or CF.

Molecule–Solvent Interaction Parameter, χ		
Molecule	2-MeTHF	CF
PM7-D3/D5	4.51	2.24
Y12	0.68	0.36
PTI04	0.70	0.36
DTY6	0.70	0.44

4. Fabrication and characterization of OPV devices

4.1. Recent green solvent processing OPVs

Table S4. Photovoltaic parameters of green solvent-treated organic solar cells under simulated solar illumination (AM 1.5G, 100 mW cm^{-2}).

Materials	Solvent	V_{OC} (V)	J_{SC} (mA cm^{-2})	FF (%)	PCE_{max} (%)	Ref.
PTQ10:Y12	2-MeTHF	0.85	23.41	66	14.5	[12]
PTQ-6bO	2-MeTHF	0.97	8.2	32.4	2.7	[13]
PM6:BTP-eC9	Eu:Tet inks	0.77	24.5	69	14.4	[11]
PM6:PY-IT	Eu:Tet inks	0.92	23.8	70	15.9	[11]
PTB7-Th:IEICO-4F	Eu:Tet inks	0.69	24.7	59	10.6	[11]
P3HT:O-IDTBR	Eu:Tet inks	0.72	11.3	59	5.3	[11]
PM6:IT-4F	Eu:Tet inks	0.83	19.4	57	9.2	[11]
PM6:BO-4F	THF	0.82	26.2	72.3	15.6	[14]
P3:IT-M	2-MeTHF	0.65	7.58	42.9	2.1	[15]
P6:IT-M	2-MeTHF	0.51	5.36	37.6	1	[15]
PBDT-TS1:$PC_{71}BM$	2-methylanisole	0.79	17.4	70.4	9.7	[16]

4.2. Device fabrication and characterization

All the devices were fabricated in a conventional structure of glass/indium tin oxide (ITO, 1.5 × 1.5 cm^2)/ poly(3,4-ethylenedioxythiophene) polystyrene sulfonate (PEDOT:PSS)/active layer/ Poly[[2,7-bis(2-ethylhexyl)-1,2,3,6,7,8-hexahydro-1,3,6,8-tetraoxobenzo[lmn][3,8] phenanthroline-4,9-diyl]-2,5-thiophenediyl[9,9-bis[3'((N,N-dimethyl)-N-ethylammonium)]-propyl]-9H-fluorene-2,7-diyl]-2,5-thiophenediyl] (PNDIT-F3N-Br)/Ag. OPV devices were fabricated according to the following procedures. ITO substrates (purchased from Thin Film Devices, Inc.) were cleaned by detergent, then sequentially ultrasonicated in DI water, acetone, and isopropanol for 30 min. The substrates were dried using compressed nitrogen and placed in an oven overnight at 100 °C. After cooling down to room temperature, the ITO substrates were treated with UV-ozone for 15 minutes and a layer of poly(3,4-ethylenedioxythiophene): poly(styrenesulfonate) (PEDOT:PSS, Clevios P VP Al 8043) was spin-coated at 3000 rpm for 60

s onto the ITO substrates. The substrates were then annealed in air at 150 ^{o}C for 20 minutes. Solutions (total concentration of 10 mg/mL) of D:A in a 1:1.2 weight ratio were prepared in 2-MeTHF, which was stirred and kept at 40 °C overnight inside a glovebox. Prior to spin casting, the stock solutions and the corresponding substrates were all heated up to 70 °C. On the top of the PEDOT:PSS layer, the hot solution was spin-coated at 1300 rpm to form active layers of approximately 100 nm. The film thickness was measured by an Ambios XP-100 stylus profilometer. All the films were thermally annealed at 110 °C for 10 minutes. After settling the films to cool to room temperature, 0.5 mg/mL PNDIT-F3N-Br solution dissolved in methanol was spin-coated on top of the active layer as a 5 nm interface layer. The Ag (100 nm) electrode with an active area of 0.05 cm^2 was then deposited on top of the active layer by thermal evaporation in a high vacuum ($<10^{-6}$ torr).

All the photoresponse and electrical measurements were conducted inside a glovebox under a nitrogen atmosphere. *J-V* characteristics were measured with a high-quality optical fiber to guide the light from the solar simulator equipped with a Keithley 2635A source measurement unit. Illuminated *J-V* curves were measured under AM 1.5G illumination (100 mW cm^{-2}). Neutral filters were applied to reach lower light intensities (10, 25, 40, 50 mW·cm^{-2}). EQE measurements were conducted with an EQE system, in which the monochromatic light intensity was calibrated using a commercial Si photodiode (Newport 818-UV). The spectral distributions of the real and imaginary components of the impedance of all devices were measured by an impedance analyzer (Solartron SI 1260A) in the dark and under illumination. To prevent the effect of the AC signal on the impedance during the measurement, a small amplitude AC signal (40 mV) was applied.

4.3. Differential Pulse Voltammetry (DPV) Measurements

Electrochemical differential pulse voltammetry (DPV) measurements were performed using a 2 mV step size, 80 ms step time and 50 mV pulse amplitude. The voltammetry experiments were performed in a glove box using a standard three-electrode cell on a 0.07 cm^2 glassy carbon button working electrode, an Ag/Ag^+ (10 mM $AgNO_3$) reference electrode and a platinum flag counter electrode. Polymer films and NFA films were drop casted from a 1 mg/mL chloroform solution onto the working electrode and allowed to air dry. Electrochemical experiments were performed using dry acetonitrile with a TBAPF6 supporting electrolyte at a concentration of 0.5 M in an

argon filled glovebox. Ferrocene/ferrocenium (−5.12 V vs vacuum) was used as an internal standard calibrated against the Ag/Ag^+ reference electrode ($E_{1/2}$ = 85 mV).

5. Morphology characterization

5.1. Topographic Characterization by Atomic Force Microscopy (AFM)

AFM images were obtained with an Asylum Research MFP-3D setup with Si probe with a resonant frequency of ~75 kHz and a force constant of 3 N m^{-1}, purchased from Budget Sensors. All measurements were carried out under nitrogen in a glove box. AFM images of the electrodes were collected with an Innova AFM setup in tapping mode.

5.2. Grazing-Incidence Wide-Angle X-ray Scattering (GIWAXS)

PLS-II 3C beamline of the Pohang Accelerator Laboratory (PAL) in the Republic of Korea was used to perform the two-dimensional (2D) GIWAXS measurements. 2D-GIWAXS images were collected at 11.57 keV (λ = 1.07156 Å) with an Eiger 4M detector (sample-to-detector distance: 414.58 mm). The incidence angle (α_i) of the X-ray beam was set between the critical angles of the thin film and substrate.

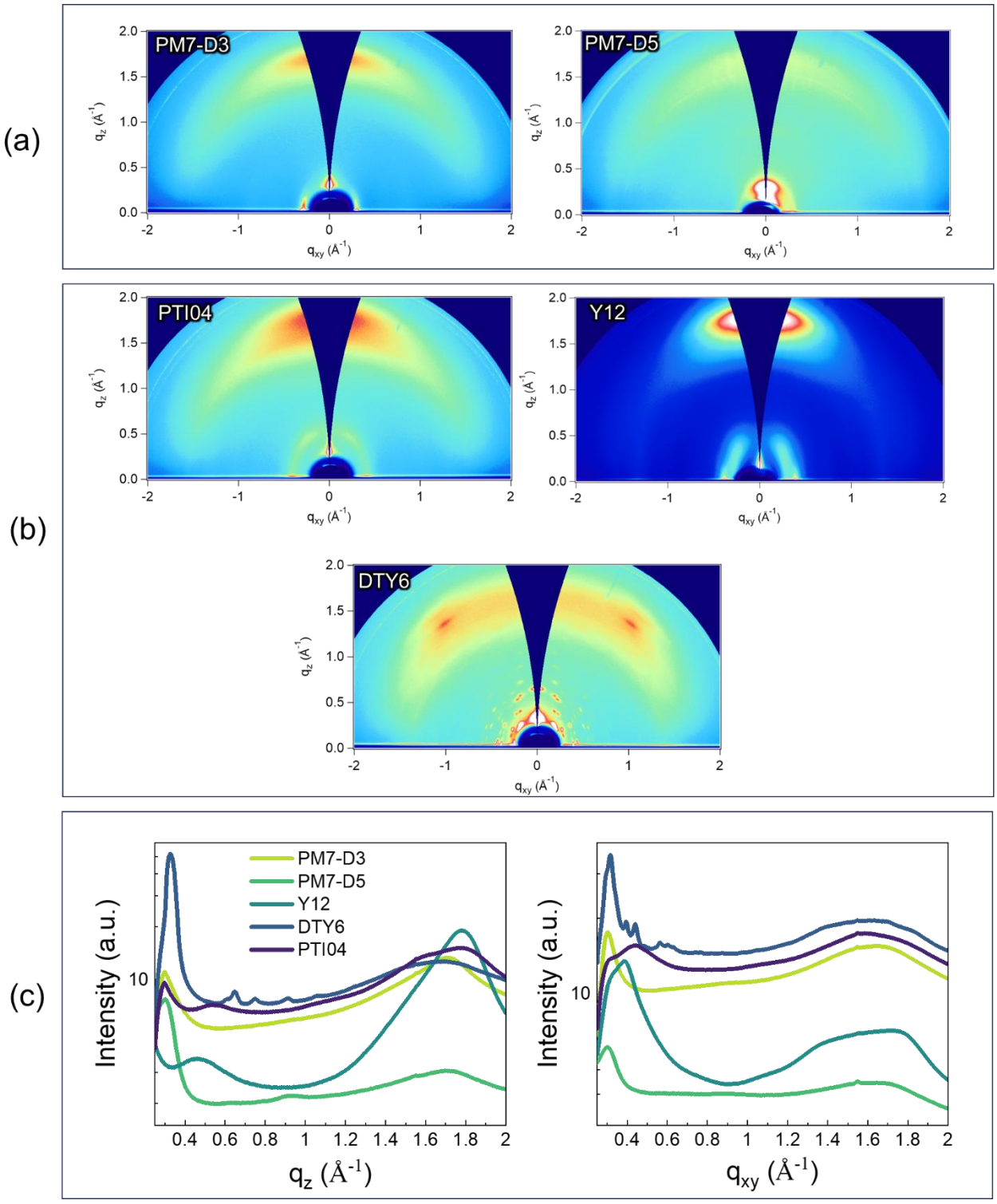

Figure S16. 2D GIWAXS patterns of the neat (a) donor, (b) acceptor films, and (c) their line cuts.

Table S5a. GIWAXS analysis of polymer:NFA blends in out-of-plane orientation (Face-on)

out-of-plane		**Peak ($Å^{-1}$)**	**FWHM ($Å^{-1}$)**	**Lattice (nm)**	**C_L (nm)**
PM7-D3:PTI04	PM7-D3 (100)	0.29	0.040	2.13	14.13
	PTI04	0.51	0.267	1.24	2.12
	π-π (010)	1.76	0.316	0.36	1.79
PM7-D3:Y12	Y12	0.36	0.063	1.75	8.95
	π-π (010)	1.77	0.270	0.36	2.09
PM7-D3:DTY6	π-π (010)	1.77	0.270	0.36	2.09
	DTY6	0.37	0.066	1.72	8.54
	DTY6	0.45	0.030	1.41	18.61
	DTY6	0.66	0.030	0.95	18.77
	DTY6	0.84	0.036	0.75	15.74
	π-π (010)	1.71	0.174	0.37	3.25
	π-π (010)	1.83	0.222	0.34	2.55
PM7-D5:PTI04	PM7-D5 (100)	0.31	0.069	2.04	8.14
	PTI04	0.52	0.228	1.20	2.48
	π-π (010)	1.77	0.313	0.35	1.81

Table S5b. GIWAXS analysis of polymer:NFA blends in-plane orientation (Edge-on)

in-plane		**Peak ($Å^{-1}$)**	**FWHM ($Å^{-1}$)**	**Lattice (nm)**	**C_L (nm)**
PM7-D3:PTI04	PM7-D3 (100)	0.31	0.056	2.06	10.07
	PTI04	0.36	0.096	1.77	5.89
	PTI04	0.45	0.198	1.39	2.86
	π-π (010)	1.73	0.478	0.36	1.18
PM7-D3:Y12	PM7-D3 (100)	0.31	0.049	2.03	11.65
	Y12	0.44	0.169	1.43	3.35
	π-π (010)	1.75	0.330	0.36	1.71
PM7-D3:DTY6		0.29	0.031	2.20	18.46
	PM7-D3 (100)	0.31	0.025	2.00	22.69
	DTY6	0.40	0.035	1.57	16.32
	DTY6	0.44	0.035	1.42	16.10
	DTY6	0.50	0.037	1.26	15.18
	DTY6	0.56	0.015	1.13	38.13
	DTY6	0.58	0.167	1.09	3.38
	DTY6	0.63	0.020	0.99	27.91
	π-π (010)	1.72	0.398	0.37	1.42
PM7-D5:PTI04	PM7-D5 (100)	0.30	0.042	2.07	13.46
	PTI04	0.34	0.074	1.87	7.65
	PTI04	0.42	0.143	1.52	3.95
	PTI04	0.89	0.058	0.70	9.70
	π-π (010)	1.77	0.383	0.36	1.48

5.3. Resonance Soft X-ray Scattering (RSoXS)

All RSoXS measurements were performed at the Advanced Light Source at Lawrence Berkeley National Lab on the 11.0.1 beamline following the previously established protocols.[17] The samples were performed in a transmission geometry with linearly polarized photons under high vacuum ($<10^{-7}$ torr) and two-dimensional scattering patterns were collected on a cooled (−45 °C) CCD with PS300 used for geometry calibration. The Nika software package for Igor (by Wavemetrics) were used for data processing. Long period estimated by RSoXS measurements and analysis are presented in **Table S6.**

Table S6. Domain size estimation by RSoXS measurements and analysis

	Peak 1			Peak 2			Root-mean-square composition variations
	Peak position q (nm^{-1})	**Long period** (nm)	Volume fraction	Peak position q (nm^{-1})	**Long period** (nm)	Volume fraction	
PM7-D3:PTI04	0.025	126	31%	0.124	26	69%	0.96
PM7-D3:Y12	0.014	225	37%	0.062	51	63%	0.63
PM7-D3:DTY6	0.015	210	44%	0.186	17	56%	0.9
PM7-D5:PTI04	0.021	150	74%	0.110	29	26%	1.0

5.4. X-ray photoelectron spectroscopy (XPS)

All XPS measurements were obtained using a Kratos Axis Ultra DLD XPS under high vacuum ($<10^{-8}$ Torr) using monochromated X-rays produced using an aluminum source running at a potential of 14 kV. A pass energy of 20 was used for all high-resolution element sweeps. The BHJ samples were prepared with the same procedure as the device fabrication. The films were mounted onto a sample bar using double-sided tape, and electrically grounded to the sample bar using nickel

impregnated tape. Data analysis was performed using CasaXPS software licensed to UCSB, and atomic sensitivity factors for each element were considered by CasaXPS during the peak integrations.

5.5. Contact Angle Measurement (CAM)

The static contact angle was measured using the sessile droplet method in a Ramé-Hart goniometer with 0.5 mL drops (~1 mm) of water or glycerol, dispensed using a syringe pump. The corresponding images were captured with a ThorLabs Zelux camera. Results are summarized in **Figure S17**.

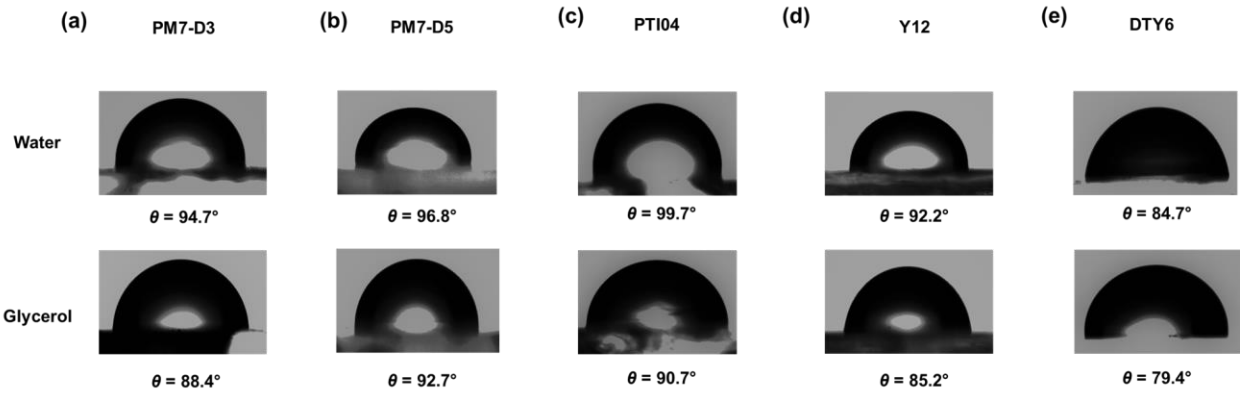

Figure S17. Water and glycerol contact angles of thin film PM7-Dx polymers and NFAs.

5.6. Flory–Huggins interaction parameter

From the water contact angle and glycerol contact angle of neat polymer and acceptor thin film (**Figure S17**), the calculation of surface tension and Flory-Huggins interaction parameters (**Table S7**) were carried out based on methodology presented in reference.[18]

Table S7. Flory–Huggins interaction parameter derived from CAM.

Blend	Flory–Huggins interaction parameter
PM7-D3:PTI04	0.036
PM7-D3:Y12	0.233
PM7-D3:DTY6	2.089
PM7-D5:PTI04	0.177

5.7. Solid-state (ss)NMR spectroscopy

For ssNMR experiments, thin-film materials were prepared by dissolving PM7-D3, PTI04, Y12, and their BHJ blends in 2-MeTHF solvents, which were spin coated on glass substrates using the same conditions used for the device fabrication. The neat and blended thin films were thermal annealed at 110 °C for 10 minutes and allowed to settle to cool to room temperature. All thin films were scratched from the glass substrates using a razor blade to collect these materials (~15 mg each) into glass vials, which were sealed with Parafilm and aluminum foil prior to shipment to the University of Lille for ssNMR studies. The neat PTI04, Y12 and PM7-D3:NFA blend materials were separately packed into 1.3 mm (outer diameter) cylindrical zirconia rotors fitted with Vespel® caps. All fast magic-angle spinning (MAS, 50 kHz) 1D ^{1}H, ^{13}C, ^{19}F, and 2D ^{1}H-^{13}C, ^{1}H-^{1}H and ^{19}F-^{19}F NMR experiments were carried out on a Bruker AVANCE NEO (18.8 T, Larmor frequencies were ^{1}H = 800.1 MHz, ^{19}F = 752.9 MHz, ^{13}C = 201.2 MHz) spectrometer with a 1.3 mm H-X probehead. The ^{1}H and ^{13}C spectra were calibrated with respect to neat TMS using adamantane as an external reference (^{13}C resonance, 35.8 ppm, and the ^{1}H resonance, 1.85 ppm),

and ^{19}F MAS spectra were calibrated to the ^{19}F chemical shift of Teflon at −132 ppm, in turn calibrated using neat $CFCl_3$ (^{19}F, 0 ppm) as an external reference.

For the neat compounds and blends, 1D ^{1}H MAS NMR experiments were carried out by co-adding 32 transients with a ^{1}H interscan delay of 4 seconds, and ^{19}F spectra were acquired with 256 co-added transients, using an interscan delay of 10 seconds. 1D $^{1}H \rightarrow {}^{13}C$ Cross Polarization (CP)-MAS NMR spectra of neat were acquired with 2048 co-added transients for neat compounds, and 4096 transients were co-added for the blend films. The CP contact time was 4 ms. The ^{1}H-^{1}H Double-Quantum–Single-Quantum (DQ-SQ) spectra of neat compounds and blends were acquired using Back-to-Back (BaBa) sequence at fast MAS:[19-21] 2D spectra were acquired with 116 t_1 increments, each with co-addition of 32 transients, to construct the vertical DQ dimension using STATES method. The ^{1}H-detected 2D ^{1}H–^{13}C HETCOR spectra of neat compounds and BHJ blends were acquired with 160 t_1 increments were acquired, each with 64 co-added transients, using 4 ms CP contact time. 2D ^{19}F-^{19}F spin-diffusion NMR spectra were acquired with a three-pulse noesy like sequence.[22, 23] For neat PTI04, Y12 and PM7-D3:Y12, 64 t_1 increments were acquired, 16 co-added transients each, using a 500 ms mixing time.

5.7.1. *Analysis of 1D ^{1}H MAS NMR spectra of neat compounds and blends*

Figure S18 compares 1D ^{1}H MAS NMR spectra of neat PM7-D3, PTI04, Y12, and PM7-D3:NFA blends, whereby the broad distribution of ^{1}H signals in the aliphatic region (0-4 ppm) correspond to distinct aliphatic proton sites which showed subtle differences in the line shapes. However, the aromatic regions in the range of 5-10 ppm showed subtle differences in the line shapes for the PM7:D3, PTI04, and Y12 molecules, suggesting the different local environments of aromatic groups. However, accurate identification of the signals corresponding to distinct aliphatic and aromatic proton sites and through-space interactions between them is not feasible due to severely overlapped signal intensities.

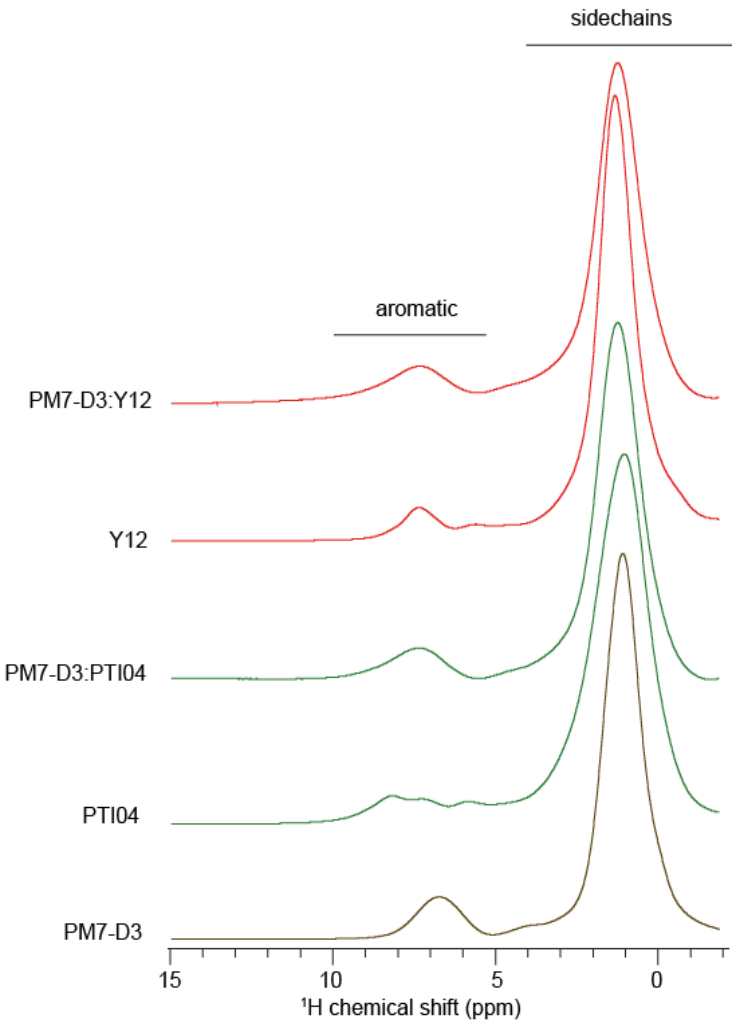

Figure S18. Solid-state 1D ^{1}H MAS NMR spectra of neat D and A compounds and PM7-D3:NFA blend films processed from 2-MeTHF. All spectra were acquired at 18.8 T (^{1}H = 800.1 MHz) with 50 kHz MAS at room temperature.

5.7.2. Analysis of 1D ^{1}H→^{13}C CP-MAS NMR spectra of neat compounds and blends

In a CP-MAS experiment, simultaneous excitation of ^{1}H and ^{13}C nuclei is carried out to achieve ^{1}H→^{13}C polarization transfer and hence ^{13}C signal intensities are enhanced. **Figure S19** shows a comparison of 1D ^{13}C{^{1}H} CP-MAS NMR spectra between neat Y12, PM7-D3, and PM7-D3:NFA blends: the signals corresponding to the distinct aliphatic and aromatic carbon sites can be identified. In the aliphatic region, ^{13}C signals at 10-16 ppm corresponds to terminal methyl groups, and signals at 20-35 ppm are attributed to central methylene groups in the linear and branched sidechains, and weak intensity signals at 35-42 ppm indicate -CH- moieties in branched

sidechains, and in the range 50-70 ppm indicate -OCH_2- groups (PM7-D3) and -NCH_2- groups (Y12).

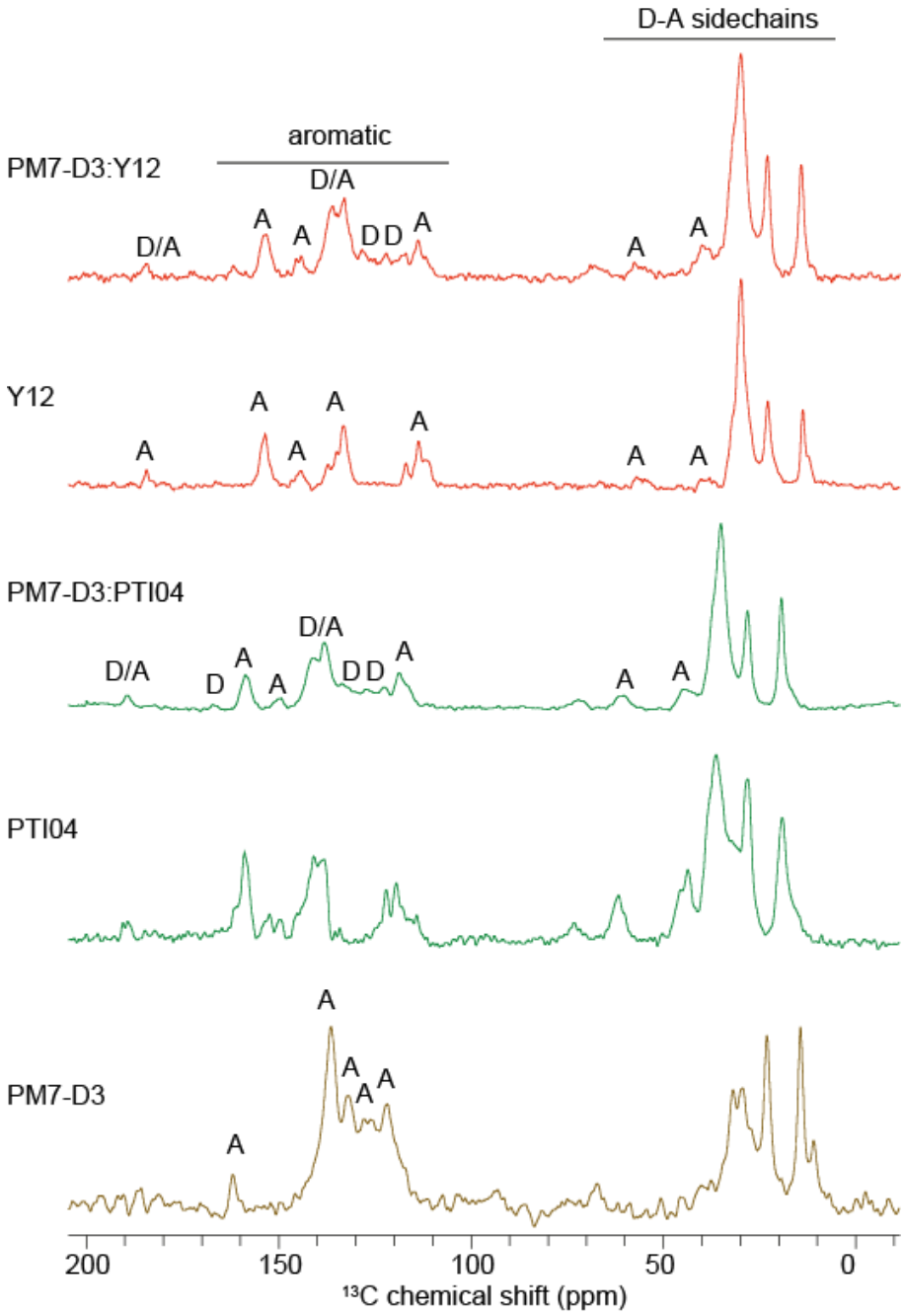

Figure S19. Solid-state 1D $^{13}C\{^1H\}$ CP-MAS spectra of neat D and A compounds, and PM7-D3:NFA blend films processed from 2-MeTHF. All spectra were acquired at 18.8 T (Larmor frequencies of ^1H and ^{13}C nuclei are 800.1 MHz and 201.2 MHz, respectively) with 50 kHz MAS.

5.7.3. Analysis of 2D ^{1}H-^{13}C and ^{19}F-^{19}F correlation spectra of neat compounds and blends

For the neat PM7-D3, PTI04, and Y12 compounds and the BHJ blends, the short-range order and intermolecular interactions are examined by analyzing the ^{1}H, ^{13}C, and ^{19}F chemical shifts and through-scape dipole-dipole interactions between them. It is noteworthy that the ssNMR magic-angle spinning (MAS) spectroscopy has been increasingly applied to characterize BHJ morphology at sub-nanometer to nanometer distances in photovoltaic blends. Although 1D ^{1}H and ^{13}C MAS spectra of neat compounds (**SI, Figures S18-S19**) provide a benchmark of different backbone and sidechain moieties in donor and acceptor molecules, the severely overlapped peaks in the analogous 1D spectra of the BHJ blends limited our resolution capabilities to accurately measure the changes in the acceptor morphology. Nonetheless, 1D ^{19}F MAS NMR enabled the local chemical environmental of ^{19}F species in the 2-(5,6-difluoro-3-oxo-2,3-dihydro-1H-inden-1-ylidene)malononitrile (2FIC) terminal groups (henceforth referred to as *end groups*) in PTI04 and Y12 molecules and their BHJ blends.[24, 25] For Y12 molecules, changes in the neat compounds and BHJ blends is evident from the changes in the ^{19}F NMR spectra patterns, while the PTI04 molecules exhibit identical local morphology in neat compounds and the BHJ blend. For the fluorinated end groups in neat PTI04 and Y12 NFAs (**Figure 5a**) and BHJ blends, the analysis of ^{19}F MAS NMR spectra are presented in **Figure 5b**. Neat Y12 processed from 2-MeTHF display ^{19}F peaks at −119 and −122 ppm, whereas the acceptor molecules in BHJ blends processed from the same solvents exhibited relatively broad peaks at −119 and −123 ppm with an additional small feature at −125 ppm. For chemically equivalent fluorine atoms in the Y12 end groups, a single ^{19}F peak is expected. The different ^{19}F peaks are due to the different intermolecular interactions between the end groups and the sidechains and the fused ring core, as previously observed for Y-series molecules.[48] The different distributions of ^{19}F signals in the ^{19}F NMR spectra of neat compounds and BHJ blends processed from different solvents indicate the presence of different local chemical environments of Y12 end groups, which were not feasible to resolve form electron microscopy, XPS and GIWAXS measurements and analyses.[26-32] Specifically, we applied extensive two-dimensional (2D) ^{19}F-^{19}F and ^{1}H-^{13}C correlation NMR spectroscopy measurements carried out at a high field (18.8 T) with fast magic-angle spinning (50 kHz MAS), which enable the D-A inter- and intramolecular interactions to be resolved and compared for the NFAs and PM7-D3:PTI04 and PM7-D3:Y12 BHJ blends (**Figure 5**). Analysis of 2D ^{19}F-^{19}F spin-diffusion (SD)

NMR spectra of PTI04 and PM7-D3:PTI04 processed from 2-MeTHF further confirms this trend (**Figures 5c** and **5d)**, whereby both materials exhibited identical spectral patterns. In such experiments, spin magnetization exchange is allowed to occur between through-space dipolar coupled ^{19}F sites, which can be adjusted by a spin diffusion time. An ensemble of closely proximate but chemically distinct ^{19}F spins within a few nanometers distance produce cross peaks (i.e., off-diagonal) in the 2D SD spectra, while the chemical shifts are detected on the diagonal. Specially, cross peaks are observed between −119 and −122 ppm, owing to the magnetization exchange between the two adjacent ^{19}F atoms in the same end group but involved in different inter- and intramolecular interactions. This indicates that the local structures of the fluorinated pendant units of PTI04 are not substantially influenced by the processing with 2-MeTHF in BHJ film formation. The identical cross peaks in the neat PTI04 and PM7-D3:PTI04 blend films clearly indicate that the nanoscale local morphology of PTI04 in the BHJ blend is retained the same as the neat compounds. The strong inter- and intramolecular interactions between the end-groups and sidechains of PTI04, especially the favorable length of branched sidechains help in maintaining the self-assembly of PTI04 molecules, resulting in the acceptor morphology to be intact in both neat compounds as well as the BHJ blends. This is particualry important for the π–π stacking interactions between the end groups (See Ref. 19, SI, Figure S17) of NFAs and the π–π overlap between the core-end groups and the assocaited charge transfer integrals that lead to efficient charge transport in acceptor regions. Crystal structures highlighting these interactions are presented in our previous study and detailed NMR crystallography analysis of these interactions are provided (Ref. 19). In contrast to this, subtle structural changes in the vicinities of end groups and sidechains are observed in Y12 molecules and the PM7-D3:Y12 BHJ blend, as evident from the similar 2D ^{19}F-^{19}F SD NMR measurements and analysis presented in **Figures 5e** and **5f**. The end group tilting in perturns the local π–π stacking interactions, which inturn perturb the charge transport. The results are corroborated by the detailed 2D ^{1}H-^{13}C and ^{1}H-^{1}H NMR measurements and analysis discussed below.

For the neat compounds and PM7-D3:PTI04 and PM7-D3:Y12 BHJ blend films cast from 2-MeTHF, **Figure 5g-j** compare the 2D ^{1}H-^{13}C HETCOR spectra. For neat PTI04 processed from 2-MeTHF (**Figure 5g**), the 2D correlation peaks at 6-8 ppm (^{1}H) and 110-125 ppm (^{13}C) corresponding to the directly bonded C-H moieties in the end groups (green) aromatic core and the 2D peaks 6-8 ppm (^{1}H) and 110-125 ppm (^{13}C) are due to the C-H moieties at the bridged

position (purple dots), and the quaternary carbon atoms in the core (thiophane (T) and benzodithiophene (BDT) moieties) were detected, and 2D peaks at ~1.0 ppm (^{1}H) and 12-15 ppm (^{13}C), and at 1.5 ppm (^{1}H) and 20-35 ppm (^{13}C) correspond to the inter- and intramolecular dipolar-coupled C-H moieties in the branched sidechains (orange and magenta dots). The 2D peaks representative of PTI04 local morphology are also presented in the PM7-D3:PTI04 BHJ blend processed from 2-MeTHF (green shaded regions), although the additional 2D correlation peaks originating from the PM7-D3 donor polymer also appear in this case as indicated by 'D' in the vertical ^{13}C axis, which is in line with the comparison of 1D ^{13}C CP-MAS NMR spectra (**SI, Figure S19**). On the other hand, neat Y12 film obtained from 2-MeTHF, the well-resolved 2D peaks associated at 110-115 ppm (^{13}C) and 6-8 ppm (^{1}H) correspond to the ^{13}C-^{1}H moieties in difluorinated indene (end groups), and the peak at 130-135 ppm (^{13}C) and 6-8 ppm (^{1}H) correspond to the -CH- in bridging position between the fused-ring core and the indene groups, as depicted in the red shaded regions. In the case of the PM7-D5:Y12 BHJ blend processed from 2-MeTHF, the 2D correlation peaks associated with the Y12 exhibited different frequencies and lineshapes as indicated by the dashed ovals, which is in line with the 2D ^{19}F-^{19}F SD measurements and analysis.

5.7.4. Analysis of 2D ^{1}H-^{1}H DQ-SQ correlation of neat compounds and blends

2D ^{1}H-^{1}H DQ-SQ correlation experiment involves the indirect excitation of DQ signals for through-space dipole-dipole coupled ^{1}H-^{1}H pairs in less than 0.5 nm, followed by a reconversion process into the direct detection of SQ coherences. As a result, a 2D DQ-SQ spectrum contains on-diagonal and off-diagonal correlation peaks with DQ and SQ peaks displayed in the horizontal and vertical axes, respectively. Specifically, DQ chemical shifts in the vertical axis resonate at the sum of the SQ chemical shifts leading to enhanced resolution in the DQ dimension, which allows the on-diagonal and off-diagonal peaks to be distinguished and identified. The off-diagonal 2D correlation peaks (also referred to as cross peaks) correspond to the through-space ^{1}H-^{1}H proximities between chemically inequivalent protons. Analysis of DQ and SQ peak facilitate the elucidation of local structures and interactions between D and A moieties in neat compounds and BHJ blends.[33]

Figure S20 presents 2D ^{1}H-^{1}H DQ-SQ spectra of neat PTI04, Y12 and PM7-D3:NFA BHJ blend films processed from 2-MeTHF solvent. For neat compounds and blends, broad distributions of ^{1}H DQ signals along the diagonal in the range of 1-8 ppm (yellow ovals) are attributable to the

through-space inter- and intramolecular ^{1}H-^{1}H dipolar interactions in the branched alkyl sidechains (see **Figure S20a**, inset). Of particular interest is the off-diagonal ^{1}H DQ signals in the range of 5-12 ppm highlighted in blue, which originate from the through-space inter- and intramolecular ^{1}H-^{1}H dipolar interactions in the branched alkyl sidechains and aromatic protons in thiophene (T), benzodithiophene (BDT) and moieties of PM7-D3 polymer, and between the sidechains and the end groups in PTI04 and Y12 moieties (yellow dots and green/red hexagons). Interestingly, the DQ peaks (red arrows) associated with the -COO-CH_2- groups of PM7-D3 (purple dots) are appeared in both neat films and in the BHJ blend films suggest the structural integrity of the sidechains, further conforming the identical local morphology in the neat compounds and blend films. Such peaks are not detected for the NFAs (dashed red circles) In addition, the on-diagonal ^{1}H DQ signals in the range of 11-16 ppm are attributable to the through-space inter- and intramolecular ^{1}H-^{1}H dipolar interactions in the aromatic moieties in PM7-D3 (T and BDT groups) and NFAs (end groups). Due to the overlapped DQ and SQ peaks in the aromatic regions, it was not feasible to resolve the structural changes in the end groups using this technique.

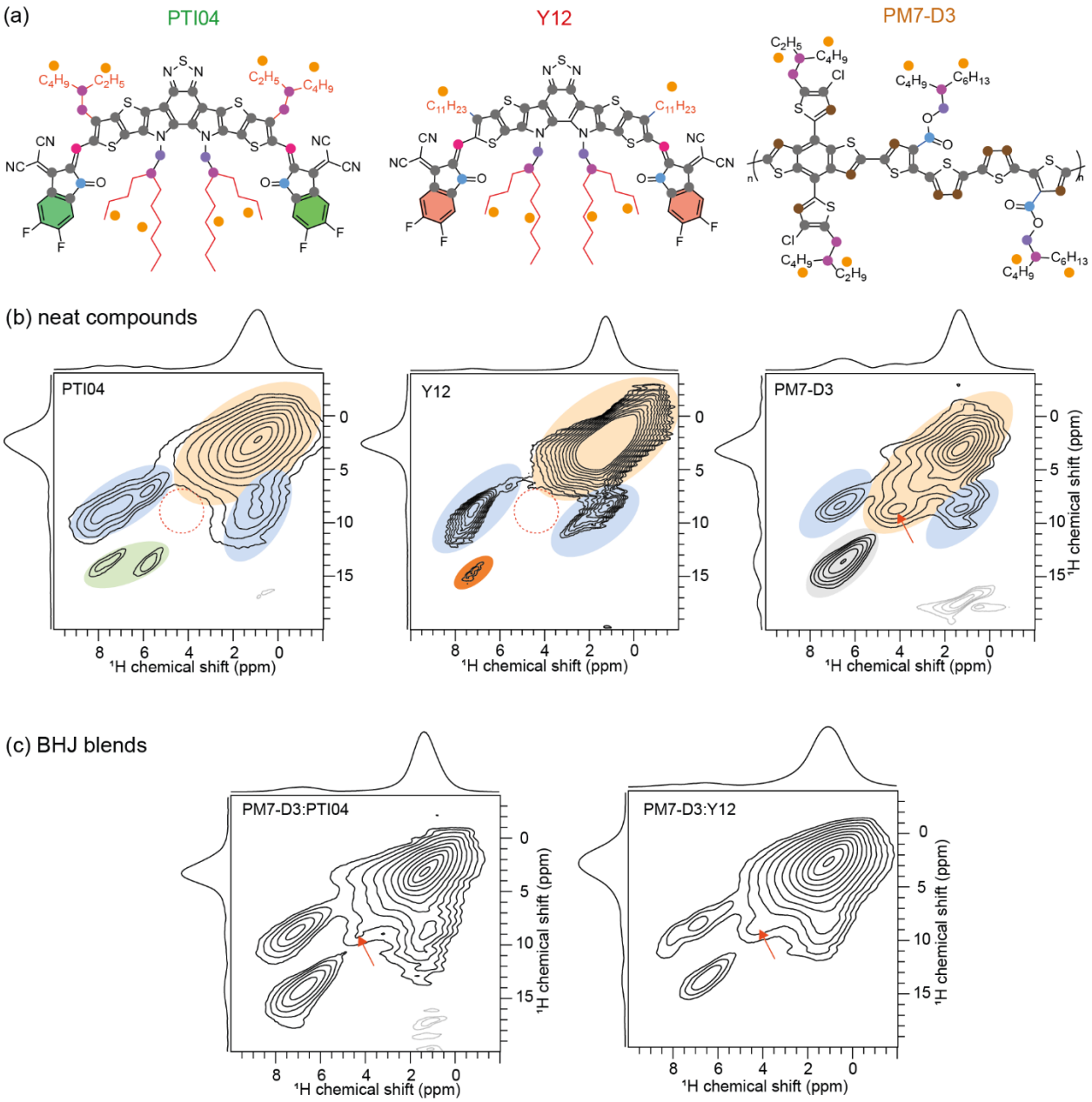

Figure S20. Solid-state 2D ^{1}H-^{1}H DQ-SQ correlation NMR spectra of neat compounds and PM7-D3:NFA blends processed from 2-MeTHF. Spectra were acquired at 18.8 T with 50 kHz MAS.

Table S8. Summarized abbreviation and full names

Abbreviation	Full name

PPDPP	Poly[(5,15-diethynyl-10,20-bis(3,4,5-tris((2-butyloctyl)oxy)phenyl) porphyrin zinc(II) complex)-alt-(2,5-bis(2-ethylhexyl)-3,6-di(thiophen-2-yl)-2,5-dihydropyrrolo[3,4-c]pyrrole-1,4-dione])]
PC71BM	[6,6]-Phenyl-C71-butyric acid methyl ester
PTzBiSi	Poly[[2,5,6,7-tetrahydro-5,7-dioxo-2-[6-[1,3,3,3-tetramethyl-1-[(trimethylsilyl)oxy]-1-disiloxanyl]hexyl]pyrrolo[3,4-f]benzotriazole-4,8- diyl]-2,5-thiophenediyl[4,8-bis[5-(2-ethylhexyl)-2-thienyl]benzo[1,2- b:4,5-b']dithiophene-2,6-diyl]-2,5-thiophenediyl]
N2200	Poly{[N,N'-bis(2-octyldodecyl)-naphthalene-1,4,5,8-bis(dicarboximide)-2,6-diyl]-alt-5,5'-(2,2'-bithiophene)}
PTQ10	Poly[[6,7-difluoro[(2-hexyldecyl)oxy]-5,8-quinoxalinediyl]-2,5-thiophenediyl]
FO6-T	Poly[(4,7-(5-fluoro-6-((2-hexyldecyl)oxy)benzo[c][1,2,5]thiadiazole))-alt-(2,5-thiophene)]
PM6	Poly[(2,6-(4,8-bis(5-(2-ethylhexyl-3-fluoro)thiophen-2-yl)-benzo[1,2-b:4,5-b']dithiophene))-alt-(5,5-(1',3'-di-2-thienyl-5',7'-bis(2-ethylhexyl)benzo[1',2'-c:4',5'-c']dithiophene-4,8-dione)]
Y6	2,2'-((2Z,2'Z)-((12,13-bis(2-ethylhexyl)-3,9-diundecyl-12,13-dihydro-[1,2,5]thiadiazolo[3,4-e]thieno[2",3":4',5']thieno[2',3':4,5]pyrrolo[3,2-g]thieno[2',3':4,5]thieno[3,2-b]indole-2,10-diyl)bis(methaneylylidene))bis(5,6-difluoro-3-oxo-2,3-dihydro-1H-indene-2,1-diylidene))dimalononitrile
PM7-D5	Poly[(2,6-(4,8-bis(4-chloro-5-(2-ethylhexyl)thiophen-2-yl)benzo[1,2-b:4,5-b']dithiophene)-alt-(5,5"'-bis(2-butyloctyl) [2,2':5',2":5",2"'-quaterthiophene]-3',4"-dicarboxylate)]
PM7-D3	Poly[(2,6-(4,8-bis(4-chloro-5-(2-ethylhexyl)thiophen-2-yl)benzo[1,2-b:4,5-b']dithiophene)-alt-(5,5"'-bis(2-butyloctyl) [2,2':5',2":5",2"'-quaterthiophene]-3,3"'-dicarboxylate)]
Y12	2,2'-((2Z,2'Z)-((12,13-bis(2-butyloctyl)-3,9-diundecyl-12,13-dihydro-[1,2,5]thiadiazolo[3,4-e]thieno[2",3":4',5']thieno[2',3':4,5]pyrrolo[3,2-g]thieno[2',3':4,5]thieno[3,2-b]indole-2,10-diyl)bis(methaneylylidene))bis(5,6-difluoro-3-oxo-2,3-dihydro-1H-indene-2,1-diylidene))dimalononitrile
DTY6	2,2'-((2Z,2'Z)-((12,13-bis(2-decyltetradecyl)-3,9-diundecyl-12,13-dihydro-[1,2,5]thiadiazolo[3,4-e]thieno[2",3":4',5']thieno[2',3':4,5]pyrrolo[3,2-g]thieno[2',3':4,5]thieno[3,2-b]indole-2,10-diyl)bis(methaneylylidene))bis(5,6-difluoro-3-oxo-2,3-dihydro-1H-indene-2,1-diylidene))dimalononitrile
PTI04	2,2'-((2Z,2'Z)-((12,13-bis(2-butyloctyl)-3,9-bis(2-ethylhexyl)-12,13-dihydro-[1,2,5]thiadiazolo[3,4-e]thieno[2",3":4',5']thieno[2',3':4,5]pyrrolo[3,2-g]thieno[2',3':4,5]thieno[3,2-b]indole-2,10-diyl)bis(methaneylylidene))bis(5,6-difluoro-3-oxo-2,3-dihydro-1H-indene-2,1-diylidene))dimalononitrile

6. References

1. A. L. Jones, C. H. Y. Ho, P. R. Riley, I. Angunawela, H. Ade, F. So and J. R. Reynolds, *Journal of Materials Chemistry C*, 2020, **8**, 15459-15469.
2. S. Li, W. Zhao, J. Zhang, X. Liu, Z. Zheng, C. He, B. Xu, Z. Wei and J. Hou, *Chemistry of Materials*, 2020, **32**, 1993-2003.
3. N. Schopp, S. Sabury, T. Chaney, J. Zhang, H. Wakidi, B. M. Kim, R. Sankar, H. M. Luong, P. Therdkatanyuphong, V. V. Brus, S. Marder, M. F. Toney, J. R. Reynolds and T.-Q. Nguyen, *ACS Energy Letters*, 2023, **8**, 3307-3313.
4. K. Jiang, Q. Wei, J. Y. L. Lai, Z. Peng, H. K. Kim, J. Yuan, L. Ye, H. Ade, Y. Zou and H. Yan, *Joule*, 2019, **3**, 3020-3033.
5. J.-D. Chai and M. Head-Gordon, *Physical Chemistry Chemical Physics*, 2008, **10**, 6615-6620.
6. R. Ditchfield, W. J. Hehre and J. A. Pople, *The Journal of Chemical Physics*, 1971, **54**, 724-728.
7. B. Mennucci, *Wiley Interdisciplinary Reviews: Computational Molecular Science*, 2012, **2**, 386-404.
8. M. J. Frisch, G. W. Trucks, H. B. Schlegel, G. E. Scuseria, M. A. Robb, J. R. Cheeseman, G. Scalmani, V. Barone, G. A. Petersson, H. Nakatsuji, X. Li, M. Caricato, A. V. Marenich, J. Bloino, B. G. Janesko, R. Gomperts, B. Mennucci, H. P. Hratchian, J. V. Ortiz, A. F. Izmaylov, J. L. Sonnenberg, Williams, F. Ding, F. Lipparini, F. Egidi, J. Goings, B. Peng, A. Petrone, T. Henderson, D. Ranasinghe, V. G. Zakrzewski, J. Gao, N. Rega, G. Zheng, W. Liang, M. Hada, M. Ehara, K. Toyota, R. Fukuda, J. Hasegawa, M. Ishida, T. Nakajima, Y. Honda, O. Kitao, H. Nakai, T. Vreven, K. Throssell, J. A. Montgomery Jr., J. E. Peralta, F. Ogliaro, M. J. Bearpark, J. J. Heyd, E. N. Brothers, K. N. Kudin, V. N. Staroverov, T. A. Keith, R. Kobayashi, J. Normand, K. Raghavachari, A. P. Rendell, J. C. Burant, S. S. Iyengar, J. Tomasi, M. Cossi, J. M. Millam, M. Klene, C. Adamo, R. Cammi, J. W. Ochterski, R. L. Martin, K. Morokuma, O. Farkas, J. B. Foresman and D. J. Fox, *Journal*, 2016.
9. B. Walker, A. Tamayo, D. T. Duong, X. D. Dang, C. Kim, J. Granstrom and T. Q. Nguyen, *Advanced Energy Materials*, 2011, **1**, 221-229.
10. D. T. Duong, B. Walker, J. Lin, C. Kim, J. Love, B. Purushothaman, J. E. Anthony and T. Q. Nguyen, *Journal of Polymer Science Part B: Polymer Physics*, 2012, **50**, 1405-1413.
11. D. Corzo, D. Rosas-Villalva, G. Tostado-Blázquez, E. B. Alexandre, L. H. Hernandez, J. Han, H. Xu, M. Babics, S. De Wolf and D. Baran, *Nature Energy*, 2023, **8**, 62-73.
12. J. Panidi, E. Mazzolini, F. Eisner, Y. Fu, F. Furlan, Z. R. Qiao, M. Rimmele, Z. Li, X. H. Lu, J. Nelson, J. R. Durrant, M. Heeney and N. Gasparini, *Acs Energy Letters*, 2023, **8**, 3038-3047.
13. J. Neu, S. Samson, K. Ding, J. J. Rech, H. Ade and W. You, *Macromolecules*, 2023, **56**, 2092-2103.
14. J. Wan, L. Zeng, X. Liao, Z. Chen, S. Liu, P. Zhu, H. Zhu and Y. Chen, *Advanced Functional Materials*, 2022, **32**, 2107567.

15. Z. Chen, L. Yan, J. J. Rech, J. Hu, Q. Zhang and W. You, *ACS Applied Polymer Materials*, 2019, **1**, 804-814.
16. H. Zhang, H. Yao, W. Zhao, L. Ye and J. Hou, *Advanced Energy Materials*, 2016, **6**, 1502177.
17. E. Gann, A. T. Young, B. A. Collins, H. Yan, J. Nasiatka, H. A. Padmore, H. Ade, A. Hexemer and C. Wang, *Review of Scientific Instruments*, 2012, **83**, 045110.
18. L. Zhang, X. Zhu, D. Deng, Z. Wang, Z. Zhang, Y. Li, J. Zhang, K. Lv, L. Liu, X. Zhang, H. Zhou, H. Ade and Z. Wei, *Adv. Mater.*, 2022, **34**, e2106316.
19. I. Schnell and S. H. Wolfgang, *Journal of Magnetic Resonance*, 2001, **151**, 153--227.
20. H. W. Spiess, 2007, DOI: 10.1002/9780470034590.emrstm0133.pub2.
21. G. N. M. Reddy, M. Malon, A. Marsh, Y. Nishiyama and S. P. Brown, *Analytical Chemistry*, 2016, **88**, 11412-11419.
22. A. Karki, J. Vollbrecht, A. L. Dixon, N. Schopp, M. Schrock, G. N. M. Reddy and T.-Q. Nguyen, *Advanced Materials*, 2019, **31**, 1903868.
23. A. Karki, J. Vollbrecht, A. J. Gillett, S. S. Xiao, Y. Yang, Z. Peng, N. Schopp, A. L. Dixon, S. Yoon, M. Schrock, H. Ade, G. N. M. Reddy, R. H. Friend and T.-Q. Nguyen, *Energy & Environmental Science*, 2020, **13**, 3679-3692.
24. A. Karki, J. Vollbrecht, A. L. Dixon, N. Schopp, M. Schrock, G. M. Reddy and T. Q. Nguyen, *Adv. Mater.*, 2019, **31**, 1903868.
25. A. Karki, J. Vollbrecht, A. J. Gillett, S. S. Xiao, Y. L. Yang, Z. X. Peng, N. Schopp, A. L. Dixon, S. Yoon, M. Schrock, H. Ade, G. N. M. Reddy, R. H. Friend and T. Q. Nguyen, *Energy & Environmental Science*, 2020, **13**, 3679-3692.
26. F. Etzold, I. A. Howard, N. Forler, D. M. Cho, M. Meister, H. Mangold, J. Shu, M. R. Hansen, K. Müllen and F. Laquai, *Journal of the American Chemical Society*, 2012, **134**, 10569-10583.
27. N. C. Miller, E. Cho, M. J. Junk, R. Gysel, C. Risko, D. Kim, S. Sweetnam, C. E. Miller, L. J. Richter, R. J. Kline, M. Heeney, I. McCulloch, A. Amassian, D. Acevedo-Feliz, C. Knox, M. R. Hansen, D. Dudenko, B. F. Chmelka, M. F. Toney, J. L. Bredas and M. D. McGehee, *Adv. Mater.*, 2012, **24**, 6071-6079.
28. M. Seifrid, G. Reddy, B. F. Chmelka and G. C. Bazan, *Nature Reviews Materials*, 2020, **5**, 910-930.
29. Z. Du, M. Mainville, J. Vollbrecht, A. L. Dixon, N. Schopp, M. Schrock, Z. Peng, J. Huang, S. Chae, H. Ade, M. Leclerc, G. N. M. Reddy and T.-Q. Nguyen, *Solar RRL*, 2021, **5**, 2100213.
30. A. L. Jones, C. H. Y. Ho, S. A. Schneider, J. Zhang, Y. Pei, J. Wang, X. Zhan, S. R. Marder, M. F. Toney and F. So, *Chemistry of Materials*, 2022.
31. B. R. Luginbuhl, S.-J. Ko, N. A. Ran, H. Hu, S. M. Becwar, A. Karki, M. Seifrid, T. Okubo, M. Wang, H. W. Ade, B. F. Chmelka, G. C. Bazan, G. N. Manjunatha Reddy and T.-Q. Nguyen, *Solar RRL*, 2022, **6**, 2200135.
32. R. L. B, P. Raval, T. Pawlak, Z. Du, T. Wang, G. Kupgan, N. Schopp, S. Chae, S. Yoon, A. Yi, H. Jung Kim, V. Coropceanu, J. L. Bredas, T. Q. Nguyen and G. N. M. Reddy, *Adv. Mater.*, 2022, **34**, e2105943.
33. B. R. Luginbuhl, P. Raval, T. Pawlak, Z. Du, T. Wang, G. Kupgan, N. Schopp, S. Chae, S. Yoon, A. Yi, H. Jung Kim, V. Coropceanu, J.-L. Brédas, T.-Q. Nguyen and G. N. M. Reddy, *Advanced Materials*, 2022, **34**, 2105943.